Methods 118–119 (2017) 146–162

Contents lists available at ScienceDirect

Methods

journal homepage: www.elsevier.com/locate/ymeth

Structural studies of RNA-protein complexes: A hybrid approach involving hydrodynamics, scattering, and computational methods

Trushar R. Patel [a,*], Grzegorz Chojnowski [b], Astha [c], Amit Koul [d], Sean A. McKenna [d,e,f,*], Janusz M. Bujnicki [c,g,*]

[a] Alberta RNA Research and Training Institute, Department of Chemistry & Biochemistry, University of Lethbridge, 4401 University Drive, Lethbridge, Alberta T1K 3M4, Canada
[b] European Molecular Biology Laboratory (EMBL) Hamburg Outstation, c/o DESY, Notkestrasse 85, Hamburg 22607, Germany
[c] Laboratory of Bioinformatics and Protein Engineering, International Institute of Molecular and Cell Biology in Warsaw, ul. Ks. Trojdena 4, 02-109 Warsaw, Poland
[d] Department of Chemistry, University of Manitoba, 144 Dysart Road, Winnipeg, Manitoba R3T 2N2, Canada
[e] Manitoba Institute for Materials, University of Manitoba, 144 Dysart Road, Winnipeg, Manitoba R3T 2N2, Canada
[f] Department of Biochemistry and Medical Genetics, University of Manitoba, 144 Dysart Road, Winnipeg, Manitoba R3T 2N2, Canada
[g] Laboratory of Bioinformatics, Institute of Molecular Biology and Biotechnology, Faculty of Biology, Adam Mickiewicz University, ul. Umultowska 89, 61-614 Poznan, Poland

ARTICLE INFO

Article history:
Received 29 September 2016
Received in revised form 1 December 2016
Accepted 5 December 2016
Available online 8 December 2016

Keywords:
Analytical ultracentrifugation
Computational modeling
Disordered and flexible systems
Dynamic light scattering
Size exclusion chromatography
Size exclusion chromatography coupled to multi-angle laser light scattering
Small angle neutron scattering
Small angle X-ray scattering

ABSTRACT

The diverse functional cellular roles played by ribonucleic acids (RNA) have emphasized the need to develop rapid and accurate methodologies to elucidate the relationship between the structure and function of RNA. Structural biology tools such as X-ray crystallography and Nuclear Magnetic Resonance are highly useful methods to obtain atomic-level resolution models of macromolecules. However, both methods have sample, time, and technical limitations that prevent their application to a number of macromolecules of interest. An emerging alternative to high-resolution structural techniques is to employ a hybrid approach that combines low-resolution shape information about macromolecules and their complexes from experimental hydrodynamic (*e.g.* analytical ultracentrifugation) and solution scattering measurements (*e.g.*, solution X-ray or neutron scattering), with computational modeling to obtain atomic-level models. While promising, scattering methods rely on aggregation-free, monodispersed preparations and therefore the careful development of a quality control pipeline is fundamental to an unbiased and reliable structural determination. This review article describes hydrodynamic techniques that are highly valuable for homogeneity studies, scattering techniques useful to study the low-resolution shape, and strategies for computational modeling to obtain high-resolution 3D structural models of RNAs, proteins, and RNA-protein complexes.

Contents

* Corresponding authors at: Alberta RNA Research and Training Institute, Department of Chemistry & Biochemistry, University of Lethbridge, 4401 University Drive, Lethbridge, Alberta T1K 3M4, Canada (T.R. Patel). Department of Chemistry, University of Manitoba, 144 Dysart Road, Winnipeg, Manitoba R3T 2N2, Canada (S.A. McKenna). Laboratory of Bioinformatics and Protein Engineering, International Institute of Molecular and Cell Biology in Warsaw, ul. Ks. Trojdena 4, 02-109 Warsaw, Poland (J.M. Bujnicki).

E-mail addresses: trushar.patel@uleth.ca (T.R. Patel), gchojnowski@gmail.com (G. Chojnowski), abhu@genesilico.pl (Astha), koula@myumanitoba.ca (A. Koul), sean.mckenna@umanitoba.ca (S.A. McKenna), iamb@genesilico.pl (J.M. Bujnicki).

http://dx.doi.org/10.1016/j.ymeth.2016.12.002
1046-2023/

1. Introduction

RNA-protein interactions play fundamental roles in many biological processes, such as regulation of gene expression, RNA splicing, and protein synthesis. The understanding of these processes improves as new structures of RNA-protein complexes are solved and the molecular details of interactions analyzed. As of November 2016, 1880 macromolecular complexes involving both protein and RNA components were available in the Protein Data Bank (PDB), including 1495 solved by X-ray crystallography, 111 by Nuclear Magnetic Resonance (NMR) spectroscopy, 269 by cryo-electron microscopy, and 5 by other methods. However, experimental determination of RNA-protein complex structures at high-resolution that allows the study of position, orientation and interactions of individual atoms is often time-consuming and in many cases, not possible due to sample preparation requirements. As a result, complete high-resolution structures are not yet available for many complexes that are crucial for numerous fundamental cellular processes. In addition, several proteins that interact with nucleic acids are either flexible or disordered in nature. For example, the N-terminal region of helicase RHAU that interacts with G-quadruplex is flexible [1]. The protein kinase R that interacts with viral RNA is composed of a flexible linker of ~80 amino acids that connects the double-stranded RNA binding domains with a kinase domain [2]. In addition, the HMGA2 family of proteins that binds with DNA replication fork are disordered in nature [3]. Thus, it will be very challenging to crystallize such proteins and nucleic acids-protein complexes. Furthermore, even if a high-resolution structure of such system is obtained, it may not represent the native solution conformation. Thus, studies on RNA-protein recognition and complex formation present major challenges for macromolecular structural biology requiring alternate approaches to gain structural information of macromolecular complexes.

In the absence of complete high-resolution structures, for many RNA-protein complexes, partial experimental data is available (*e.g.*, high-resolution structures of all or some isolated components). This fragmentary data can often be supplemented with low-resolution structural data that provide information about the shape or the proximities and interactions of components. Given the scarcity of experimentally determined structures of RNA-protein complexes and the wide range of heterogeneous information from biochemical and biophysical data, computational techniques can be used to integrate existing data, guide structure elucidation and subsequently determine the mechanisms of action and interactions between components. This approach is commonly called a *hybrid* or an *integrative* modeling. Theoretical models of macromolecular structures can assist in understanding and guiding the identification of important interaction surfaces and, more importantly, can provide a starting point for higher-resolution descriptions.

Typically, an RNA is prepared using an *in vitro* transcription method due to its cost-effectiveness, scalability, and often biological relevance of RNA structures over the commercially available synthetic RNA. The quality of such RNA preparations is scrutinized by means of denaturing and native polyacrylamide gel electrophoresis to ensure that the RNA is of appropriate length and that it is in a single conformation. The quality of RNA is also routinely assessed by the size exclusion chromatography [4]. On the other hand, a protein is recombinantly expressed in either bacterial or eukaryotic host, followed by purification using affinity and size exclusion chromatography. This review provides necessary information on biophysical hydrodynamic methods (analytical ultracentrifuge and dynamic/static light scattering) that are key to ensuring the suitability and quality of RNA, proteins and their complexes required for low-resolution structural studies (solution X-ray and neutron scattering). The benefits and limitations of each method in studying homogeneity, aggregation state, and low-resolution shape of macromolecules and macromolecular complexes are also discussed. Furthermore, the introduction to computational modeling methods and applications of such methods to obtain detailed 3D structural models of RNA-protein complexes are also described. More importantly, approaches to combine experimental data (low-resolution and high-resolution) on unbound RNA and proteins, as well as their complexes, with computational modeling to obtain high-resolution models of RNA-protein complexes are discussed. In summary, we provide a methodological pipeline to determine high-resolution models of RNA-protein complexes that are not suitable for structural investigation by X-ray crystallography, NMR or cryo-electron microscopy, but are amenable for low-resolution structural studies in solution (Fig. 1).

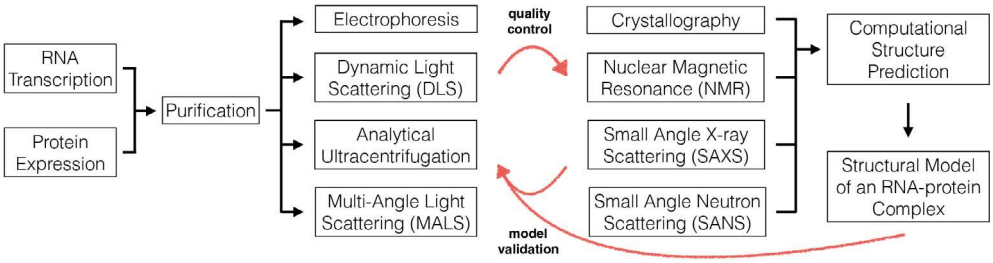

Fig. 1. Outline of a hybrid approach to study RNA-protein interactions.

2. Methods

2.1. Size exclusion chromatography

Application of size exclusion chromatography (SEC; also known as gel permeation or gel filtration chromatography) for removal of aggregated and/or degraded macromolecules to obtain a monodisperse preparation of macromolecules (proteins, RNA, DNA and their complexes) has become a routine in biochemistry and structural biology methods [1,5–8]. SEC involves a column packed with porous gel beads designed to enable separation of biomolecules based on their relative time spent sampling the pores under the constant flow of mobile phase (appropriate solvent). In a typical SEC purification step, a buffer solution containing the species of interest is applied onto the column with larger aggregates/molecules eluting in less volume than their smaller counterparts, as smaller components can enter through pores of the beads. Therefore, separation is based on the hydrodynamic properties of the macromolecules, which prepares them for subsequent analysis. Gel electrophoresis of samples is used to assay the purity of the eluted material. Highly purified preparation of macromolecules and their complexes is crucial for their biophysical characterization using the methods discussed in this review article.

2.1.1. Benefits and limitations

In principle, SEC can be used to rapidly estimate the hydrodynamic (Stokes) radius (R_h) relative to known calibration standards of similarly shaped molecules. A calibration plot is constructed from the corresponding elution volumes (V_e) for a series of proteins with known R_h (log R_h *vs.* V_e). In cases where one can assume a spherical shape, molecular weight (M_w) of macromolecules can also be estimated [9–12]. Ideally, the calibration plot should be expressed in terms of the R_h and not M_w [11–14] due to the fact that the macromolecules are rarely spherical. For example, elongated macromolecules such as RNA stem-loops typically display significantly larger R_h than a protein of the same M_w [15]. Therefore, caution must be exercised while estimating R_h for macromolecules that are elongated and flexible (*e.g.*, RNA) using a calibration plot. In such cases, the dynamic light scattering (DLS) technique should be employed [16]. Additionally, V_e will change for self-associating macromolecules or for macromolecules that interact with column packing material. Therefore, while rough estimates on size can be obtained, SEC should be primarily used to obtain an aggregation/degradation-free preparation or to purify relatively stable complexes from a preparation where multiple complexes exist.

2.2. Analytical ultracentrifugation

Analytical ultracentrifugation (AUC) is widely applied in biomolecular and pharmaceutical sciences to study homogeneity, M_w, interaction studies and aggregation/stability analysis of a range of macromolecules [1,6,8,17–23]. The concept and development of the analytical ultracentrifuge (AUC) by Svedberg and co-workers nearly a century ago [24] has progressed to the modern instrument first introduced in the 1990s by Beckman Instruments (USA), with on-line data collection and computer-aided data analysis. AUC experiments can be undertaken in a wide range of solution conditions in terms of pH, ionic strength, temperature (~4–40 °C) and co-solutes allowing a complete description of a macromolecular solution characterisation/behavior to be determined under nearly physiological conditions. In addition to the information on homogeneity and on the parameters describing macromolecular size and shape, it is also possible to study interactions with ligands and self-association of macromolecules [25–33]. An outstanding feature of analytical ultracentrifugation is that all determinations (including M_w) are carried out without calibration with known standards unlike other techniques, such as SEC [34,35].

AUC relies on the separation of macromolecules according to their size and density. Both sedimentation and diffusion behaviors of macromolecules can be expressed using the *Lamm equation* [36] as:

$$\frac{\partial c}{\partial t} = \left(\frac{1}{r}\right)\left[\frac{\partial}{\partial r}\left\{rD\frac{\partial c}{\partial r}\right\} - s\omega^2 r^2 c\right] \quad (1)$$

where, c, t, r and ω represent concentration of macromolecules, time, radius and angular velocity respectively. D is the diffusion constant and s is the sedimentation coefficient: a parameter that characterizes the motion of the macromolecule in a centrifugal field. Interestingly, the first term and ($d/dr(rD.dc/dr)$) the second term ($s\omega^2r^2c$) on the right-hand side of the equation describes *diffusion* and *sedimentation* process respectively. It is therefore possible to perform two types of experiments using AUC: sedimentation velocity (AUC-SV) and sedimentation equilibrium (AUC-SE).

2.2.1. Sedimentation velocity using AUC

AUC-SV experiments provide information on size, shape, conformation and interactions of macromolecules. In a typical SV experiment, a solution containing macromolecules is spun at a high angular velocity, depending on the mass of macromolecules. Modern AUCs offer three optical systems-operate on the differential spectroscopic method to collect/record the difference in optical properties between a sample solution (containing macromolecules and solvent) and a reference solution (containing only solvent). For macromolecules with a chromophore (proteins and nucleic acids), UV/VIS absorption optics are suitable, whereas all macromolecules (including fatty acids and polysaccharides) can be studied using the Rayleigh interference (refractometric) optical system. The fluorescence detection system takes advantage of the attached fluorophore group on macromolecules and provides high-sensitivity as well as selectivity for data collection. At the beginning of the centrifugation process ($t = 0$), particles are uniformly distributed throughout the cell, but at $t > 0$ macromolecules have moved towards the bottom of the cell under the influence centrifugal force resulting into a sedimenting boundary. For a monodisperse

preparation, a single boundary is observed. During the sedimentation process, macromolecules move at constant velocity because frictional forces cause particles to quickly attain a terminal velocity [25,34]. The ratio of the velocity (v) at which the macromolecules move with respect to the centrifugal field ($\omega^2 r$) is termed as the *sedimentation coefficient, s* defined by, [37].

$$\frac{v}{\omega^2 r} = \frac{M_w(1-\bar{v}\rho)}{Nf} = s \tag{2}$$

The term $v/\omega^2 r$ is the velocity of the particle per unit gravitational acceleration can also be termed as *s* (unit of seconds, i.e. 1 S equals to 10^{-13} s), which depends on size, shape and frictional properties of macromolecules. $\bar{v}$ is the partial specific volume (which is a measure of the change in volume of a solution per gram of macromolecule in that solution [38]) in mL/g, ρ is the density in g/mL and *r* is the radius in cm. The frictional coefficient (*f*) can be defined as the proportionality of the frictional force (F) experienced by a moving particle under the influence of external force or due to Brownian motion, and the velocity (*v*) of particle.

Interestingly, both, thermodynamic and hydrodynamic information can be obtained from the sedimentation coefficient [39]. The sedimentation coefficient determined at particular experimental conditions, is denoted as $s_{T,b}$ where '*T*' is experimental temperature and '*b*' represents the solvent. Prior to reporting AUC-SV data, the sedimentation coefficient is normalized for any contributions made from solvent density and viscosity in the determination of the *s* value, to obtain a sedimentation coefficient corrected to standard solvent conditions [37].

$$s_{20,w} = s_{T,b}\left(\frac{1-\bar{v}\rho_{T,b}}{1-\bar{v}\rho_{20,w}}\right)\left(\frac{\eta_{20,w}}{\eta_{T,b}}\right) \tag{3}$$

where, $s_{20,w}$ is the sedimentation coefficient expressed in terms of the standard solvent of water at 20 °C. As the *s* value is concentration dependent, it will gradually *decrease* with increasing concentration for non-associating macromolecules due to non-ideality effects [37], which is corrected by measuring $s_{20,w}$ at different concentrations and extrapolation to infinite dilution to obtain $s^0_{20,w}$:

$$s_{20,w} = s^0_{20,w}(1-k_s c) \tag{4}$$

The $s^0_{20,w}$ represents sedimentation coefficient corrected for standard solvent conditions and for non-ideality by extrapolating $s_{20,w}$ measured at a series of concentrations and to infinite dilution ($s_{20,w}$ *vs c* plot). The concentration dependence of sedimentation coefficient, Gralén parameter k_s is typically small for globular macromolecules but much larger for random coil or elongated macromolecules such as RNA. A negative slope on this plot represents non-interacting behavior whereas the positive slope indicates self-association of macromolecules.

2.2.1.1. Benefits and limitations. Using AUC-SV, the homogeneity, self-association behavior and aggregation of macromolecules can be studied over a range of concentrations, temperatures, and buffer conditions. In addition, information on subunit stoichiometry and affinity parameters can also be gained. Furthermore, a low-resolution estimate of macromolecular (or macromolecular assembly) shape in solution can be evaluated. Conformational changes in macromolecules upon interaction with partners or due to change in solvent conditions can also be investigated using AUC-SV. AUC-SV is an ideal technique to study the quality of SEC-purified macromolecules and their complexes for structural studies using methods discussed in this review. As a negative, AUC-SV is time-consuming experiment for simple determination of aggregation. DLS is an appropriate alternative that requires significantly less time (~20 min vs 6–8 h) and sample (~10–20 μL vs 400 μL, Table 1) to evaluate the homogeneity of a wide-range of macromolecules.

Table 1
Summary of biophysical parameters that can be employed for model building and validation.

Technique	Parameters	Volume (μL)	Time
SEC	R_h	~50–100	~45 min
AUC-SV	s, M_w	~400	6–8 h
AUC-SE	M_w	~80	24–48 h
DLS	D, R_h	~10–20	~20 min
SEC-MALLS	M_w, R_g	~50–100	~1 h
SAXS	M_w, R_g, D_{max}	~15–50	10 min–1 h
SANS	M_w, R_g, D_{max}	~15–50	10 min–1 h

2.2.2. Sedimentation equilibrium using AUC

AUC-SE is a thermodynamic, as opposed to hydrodynamic, method for determination of absolute M_w of macromolecules and their complexes [25,40–43]. AUC-SE also provides information on subunit composition for multi-subunit macromolecules, an average molar mass *M* for heterogeneous systems, and determination association/dissociation constants [21,25,44,45]. AUC-SE fundamentally differs from AUC-SV in that it requires a lower rotor speed, less sample (minimum of ~80 μL vs. 400 μL for a single experiment) and more experimental time (~24–48 h vs. 6–8 h). In a typical AUC-SE experiment, a dialyzed solution of macromolecules is subjected to centrifugation at a low angular velocity. The sedimentation of macromolecules is balanced by diffusion forces from the bottom of the ultracentrifuge cell when equilibrium is reached, resulting in a steady state concentration gradient where a lower concentration of the macromolecules occurs at the meniscus, and increases continuously to a higher concentration at the bottom [46]. Thus, a time-invariant concentration gradient develops as the flux of sedimenting macromolecules is exactly balanced by the flux of opposite diffusing macromolecules at each point across the cell (*i.e.* a thermodynamic equilibrium is obtained between sedimentation and diffusion forces) [34]. The Rayleigh interference optical system can be used to gain a direct and accurate record of sample concentration where, as light waves pass through reference and sample sectors, waves undergo interference resulting in light and dark fringes because of the difference in the refractive index of sample and solvent [37]. It registers the concentration of solution at a given radial position in the cell relative to the concentration at the meniscus. For absorbance optics, an appropriate wavelength could be used to detect macromolecular concentration (*e.g.* protein and nucleic acids).

The increase in concentration gradient for a monodisperse and non-interacting, ideal macromolecular preparation can be represented as:

$$M_w(r) = \frac{\partial \ln J(r)}{d(r^2)}\frac{2RT}{(1-\bar{v}\rho)w^2} \tag{5}$$

where, $J(r) = J(a) + j(r)$. $J(r)$ is an absolute fringe concentration at the radial position *r* and is directly related to the fringe concentration relative to the meniscus $j(r)$ and absolute meniscus concentration $J(a)$.

Thus, the Rayleigh patterns can be transformed into the plot of $\ln J(r)$ vs. r^2 (or plot of $\ln c$ vs. r^2 for a UV detection system) to obtain $M_w(1-\bar{v}\rho)w^2/2RT$ as a slope that yields the M_w for monodisperse systems [47]. For heterogeneous systems, molar mass from the *average slope* will be a weight average M_w [48]. The M_w obtained using AUC-SE is known as *apparent* molecular weight ($M_{w,app}$) meaning that the molecular weight was obtained from an experiment performed at a finite concentration. Extrapolation of

apparent molecular weight measured at different concentrations to zero facilitates measurement of the *ideal* molecular weight, M_w.

2.2.2.1. Benefits and limitations. The AUC-SE is a very useful technique to study self-associating systems [26,29,49] and to obtain information on the dissociation constant, K_d, (10^{-3} to 10^{-8} M) that compares with other techniques such as isothermal titration calorimetry (10^{-6} to 10^{-11} M), fluorescence-circular dichroism-light scattering spectroscopy (10^{-6} to 10^{-11} M) and differential scanning calorimetry (10^{-9} to 10^{-20} M) [27]. Information on subunit stoichiometry, macromolecular assemblies, protein-protein complexes, protein-carbohydrate complexes and protein-nucleic acid complexes as well as equilibrium constants for hetero-associating systems can also be obtained using AUC-SE [27,46], that could be very useful for interpretation of structural-biophysical data. Thermodynamics, free energy and conformational changes can also be studied by this technique [27,50]. The main disadvantage is that AUC-SE is very time-consuming. M_w of macromolecules and their complexes can be studied more rapidly using either a combination of sedimentation velocity and dynamic light scattering methods [1,5,6,17,51,52] or using size-exclusion chromatography in combination with multi-angle laser light scattering [53–57]. For more information on AUC, readers are advised to refer additional recent review articles [17,30,58–62].

2.3. Light scattering

The foundation for the application of light scattering to study biological macromolecules was laid in the 1870s by work from John Tyndall and Lord Rayleigh [63,64]. Significant contributions from Mie and Einstein in the early 1900s, who developed Mie theory and Brownian motion/Stokes-Einstein theory respectively, further strengthened research in light scattering [65,66]. Eventually, efforts by a number of researchers led to the development of two separate fields of light scattering – dynamic light scattering (DLS) and static light scattering (SLS). The fundamental difference between the two branches of light scattering is based on the nature of the scattered light being detected. In DLS, intensity fluctuations of scattered light caused by the Brownian motion of macromolecules in solution are detected as a function of time to provide information on the diffusion behavior (and ultimately hydrodynamic size) of macromolecules [67,68]. If the detector detects the intensity of scattered light as a function of scattering angle that depends on the size and shape of macromolecules; it is termed as static light scattering. SLS provides valuable information on M_w and the radius of gyration (R_g, average root mean squared radius from the center of the mass for a macromolecule) of macromolecules [69,70]. Depending on the light source, high- or low-resolution shape information can also be obtained using SLS.

2.3.1. Dynamic light scattering

DLS, also known as photon correlation spectroscopy or quasi-elastic light scattering, measures diffusion behavior of macromolecules undergoing the Brownian motion [69,71,72]. The macromolecules are in continuous motion in solution due to the bombardment from surrounding solvent molecules. Large macromolecules diffuse slowly, resulting in a smaller diffusion coefficient, whereas small macromolecules diffuse faster resulting in higher diffusion coefficients. The diffusion coefficient (D) measured using the intensity fluctuations of light can be converted to hydrodynamic radius (R_h, radius of a hypothetical sphere that diffuses at the same rate as particle under investigation), using the Stokes-Einstein equation [73].

$$D = \frac{K_B T}{6\pi\eta R_h} \tag{6}$$

where k_B is the Boltzmann coefficient (1.380×10^{-23} kg.m^2.s^{-2}.K^{-1}), T is an absolute temperature, and η is the viscosity.

The determination of D, and therefore R_h depends on size and shape of macromolecules as well as experimental temperature and solvent viscosity [69], implying that caution should be exercised in solvent selection while performing DLS experiments. The R_h can be utilized to gain shape information of macromolecules using the following the equation [74].

$$f = 6\pi\eta R_h \tag{7}$$

where, f represents the translational frictional coefficient that can be employed to calculate frictional ratio f/f_0 (ratio of Stokes radius to that of a sphere with the volume of an unsolvated macromolecule) of macromolecules that is unity for spherical macromolecules but increases gradually for elongated and asymmetric macromolecules.

2.3.1.1. Benefits and limitations. DLS is a non-invasive, rapid, and reliable method to study homogeneity and aggregation of macromolecules and their complexes, which is very useful in preparations for solution (X-ray and neutron) scattering and X-ray crystallography studies. It offers a host of benefits that other techniques cannot provide. For example, using DLS, it is possible to study homogeneity of macromolecules at a wide range of concentrations, solvent (salt and additives) conditions and temperatures. Another advantage of DLS compared to AUC or other methods is the amount of sample required. For a typical AUC-SV experiment, ~400 μL is required, whereas DLS requires a significantly lower amount of sample (Table 1). DLS measurements are also rapid (~20 min) compared to 6–8 h of AUC-SV or ~45 min required for a typical SEC-MALLS experiment. DLS measurements at multiple temperatures also enable thermal stability studies, which is useful in comparing batch-to-batch preparations of macromolecules for consistency. However, users should also be aware of the limitations of DLS. Similar to AUC, temperature must be kept constant throughout an experiment and accurate information of solvent viscosity must be known. Extreme caution should be exercised while interpreting monomer-dimer association of macromolecules, as dimerization of macromolecules may not lead to a change in R_h that could be reliably detected. DLS is inherently biased towards dust particles and high molecular weight aggregates, therefore the samples must be filtered and cuvette must be cleaned thoroughly. For further details on DLS, readers should refer to additional review articles [16,69,75–79].

2.3.2. Size exclusion chromatography – coupled with multiangle laser light scattering

In principle, absolute M_w using light scattering can be obtained if scattering intensity is measured at either sufficiently low angles (such as SAXS) or if multi-angle detectors are used which facilitates extrapolation to low-angle intensities. The size exclusion chromatography coupled with multiangle laser light scattering (SEC-MALLS) involves combination of three techniques – size exclusion chromatography (SEC), a photometer (multi-angle light scattering detector) and a refractometer (concentration detector) [70,80,81]. In a typical SEC-MALLS instrument, separated macromolecules from SEC (based on their size) enter, via continuous flow, first into a light scattering instrument containing multiple detectors (18–20) at various angles and then to a refractive index (RI) detector. The RI detector then measures the concentration of SEC separated fractions whose M_w was determined using MALLS. In addition, it is also possible to connect the UV-detector, viscometer as well as DLS to SEC-MALLS set-up to obtain concentration using UV-absorbance method, viscosity as well as R_h of macromolecules respectively. The application of SEC is crucial as the presence of even trace amount of aggregates will lead to an overestimate of M_w. Light

scattering, like AUC-SE, is one of the few methods widely used for the *absolute* determination of M_w, mass distribution and the shape of macromolecules and their complexes [47,82–85]. SEC-MALLS has been successfully applied to study M_w and stoichiometry of proteins, RNA and their complexes [56,57,86–91] complementing structural-biophysical analysis by solution (X-ray and neutron) scattering, X-ray crystallography and NMR studies. If SEC resolution is sufficiently high, *z*-average (M_z) and number-average (M_n) molecular weights can also be estimated, which are useful parameters to study polydispersity. SEC-MALLS can also provide radius of gyration (R_g) for sufficiently large macromolecules (molecules with size >λ/20, where λ is the wavelength of the incident light). As SEC-MALLS uses laser light (wavelength of ~658 nm), R_g for biomolecules such as proteins and nucleic acids cannot be determined accurately since they are too small compared to the wavelength of the incident light. Therefore, other methods such as SAXS are employed (wavelength of ~0.1–0.3 nm) to obtain R_g for proteins, nucleic acids and their complexes (see Sections 2.3.3 and 2.3.4).

It is important to note that the amount of scattered light is directly proportional to M_w, and $(dn/dc)^2$ (refractive index increment) of macromolecules. Therefore, to determine M_w, the light scattering intensity at various angles (measured with MALLS), the concentration (c) of the macromolecules (measured by the concentration – or refractive index detector), and the specific refractive index increment (dn/dc) values of macromolecules are required. The RI detector measures dn/dv, which is the inverse of the change in voltage the refractometer produces based on the differences in refractive index between the sample and the reference. Once the dn/dv is measured, the baseline signal (v) can be converted to c by applying the dn/dc value. Typically, the dn/dc values for proteins range from 0.16 to 0.20 mL/g, for RNA from 0.17 to 0.19 mL/g and for DNA, 0.17 mL/g. The dn/dc values for many macromolecules have been provided in Thiesen et al. [92]. The Debye-Zimm method is primarily used for data analysis [93], as it relates the excess Rayleigh ratio R_θ, to concentration and weight-average molar mass to determine the M_w using following equation.

$$\frac{R_\theta}{K^* c} = M_w P(\theta) - 2A_2 c M^2 P^2(\theta) \tag{8}$$

R_θ is the excess Rayleigh ratio and A_2 is the second virial coefficient. The K^* is the optical constant, $4\pi^2 \eta_0^2 (dn/dc)^2 \lambda_0^{-4} N_A^{-1}$, where n_0 is the refractive index of the solvent, $_0$ is the incident wavelength and NA is Avogadro's number. The $P()$ $(1 - 2\mu^2 \langle R_{gz}^2 \rangle / 3! + \ldots)$ describes size, shape and structure of macromolecules where $\langle R_{gz}^2 \rangle$ represents the radius of gyration and $\mu = 4\pi(\sin\theta/2)/\lambda$. The reciprocal of equation (Zimm equation) can be expressed as:

$$\frac{K * c}{R_\theta} = \frac{1}{P(\theta)} \left(\frac{1}{M_w} + 1A_2 c \right) \tag{9}$$

Thus, a linear fit to a plot of $K^*c/R(\theta)$ *vs.* $\sin^2(\theta/2)$ is made for an ideal system to obtain M_w and $\langle R_{gz}^2 \rangle$ from the intercept and slope at zero angle respectively [74]. This approach, while popular, discards most of the higher angle data [70,94], and therefore an alternative method (Debye) [95]) that allows linear fitting of all the light scattering detector data is recommended. In Debye method, a plot of $R(\theta)/K^*c$ *vs.* $\sin^2(\theta/2)$ is constructed followed by a polynomial fit to obtain the M_w and $\langle R_{gz}^2 \rangle$ from the intercept and slope. The Debye method provides more reliable estimates of M_w and $\langle R_{gz}^2 \rangle$ over a wider range of molecular weight as compared to the Zimm formalism.

2.3.2.1. Benefits and limitations. Similar to AUC-SV and DLS, SEC-MALLS is the method of choice to assess homogeneity of individual species or complexes to ensure high-quality sample preparation prior to structural studies. Using SEC-MALLS, it is possible to obtain an absolute weight average molecular weight (M_w), radius or gyration (R_{gz}), and, the second virial coefficient (A_2). Similarities between AUC-SE and SEC-MALLS include their ability to obtain an absolute M_w in solution and non-invasive nature of both methods. However, compared to AUC-SE, a typical SEC-MALLS experiment takes ~1 h to determine the M_w. SEC-MALLS measurements can be performed under a range of solvent conditions (pH and ionic strengths), and in the presence or absence of ligands. Although the SEC column removes supramolecular contamination, it is advisable to filter the sample and/or clear large aggregates by means of centrifugation prior to light scattering analysis. As the amount of scattered light is proportional to $c.M_w$ (concentration and molecular weight), for macromolecules <50 kDa, a relatively high concentration of macromolecules is required to obtain strong signals [70,80]. Additionally, an accurate dn/dc value is also required as determination of concentration of SEC-separated fractions and of M_w is dependent on errors in $(dn/dc)^2$ [70,80]. Further details on SEC-MALLS can be found in excellent review articles: [69,80,83,96–99].

2.3.3. Small angle X-ray scattering

Small angle X-ray scattering (SAXS), also known as solution X-ray scattering, is a type of static light scattering that employs high-energy X-rays as opposed to the laser light that is being utilized in SEC-MALLS. Due to the short wavelength of X-rays (0.1–0.3 nm), molecular structure and R_g of macromolecules and their complexes can be obtained. However, in contrast to the X-ray diffraction from macromolecular crystals, only a low-resolution shape information (~10–20 Å) can be obtained using SAXS. SAXS offers the benefit of studying proteins, RNA and their complexes in solution. [60,100–104]. Therefore, for a monodisperse and non-interacting system, scattered light intensity is proportional to that from a single macromolecule averaged over all orientations.

In a typical SAXS experiment, a solution containing macromolecules is exposed to high-energy monochromatic and collimated X-rays, and the scattering intensity ($I(q)$) is detected as a function of scattering vector length (q). The high-energy low-wavelength light is able to penetrate into macromolecules and interact with the electrons resulting in elastic scattering of light based on the size and shape of macromolecules. The term 'small angle' is very critical as the detector collects data at only very small angles (~0.1–10°) that is essential to obtain reliable size and shape information [102,105,106]. Modern synchrotron facilities employ a range of sample-to-detector distances resulting in q values from ~0.02 to 8 nm^{-1}, covering an R_g range of ~1–25 nm. In-house SAXS instruments (*e.g.* Rigaku and Anthon Paar) provide measurements in the range of 0.06–6 nm^{-1}, however, in practice it is very difficult to gain reliable information beyond ~3.5 nm^{-1} using in-house sources.

The scattering vector length, q, can be defined as:

$$q = \frac{4\pi \sin\theta}{\lambda} \tag{10}$$

where 2θ is the angle between incident and scattering radiation whereas, λ is the wavelength of the incident light. SAXS data for both solvent and solvent-solute preparations are collected followed by data subtraction to eliminate scattering contributions from solvent. The resulting 1D plot represents intensity of scattered light ($I(q)$) at scattering angle (q) [102,105,106].

For a monodisperse system, the $I(q)$ depends on a form factor, $P(q)$ and structure factor, $S(q)$.

$$I(q) = n\Delta\rho^2 V^2 P(q) S(q) \tag{11}$$

where, n is the number density of macromolecules (ratio of concentration c to mass, M), $\Delta\rho$ is the difference ($\rho(r) - \rho s$) in the average electron density of solute ($\rho(r)$) and solvent (ρs), and V is the

volume of macromolecules (that is proportional to the mass, M of macromolecules). As expected, higher $\Delta\rho$ values provide better signal-to-noise ratios. Note that the nucleic acids have higher averaged density (~0.51 $e^-/Å^3$) compared to proteins (~0.44 $e^-/Å^3$) and bulk solvent (~0.33 $e^-/Å^3$), resulting in a stronger signal at similar concentrations. For monodisperse systems under dilute conditions, extrapolation of intensities of scattering light to infinite dilution leads the structure factor to become 1. Therefore, Eq. (11) can be rewritten as:

$$I(q) = cM\Delta\rho^2 P(q) \tag{12}$$

Thus, shape information for macromolecules can be obtained using form factor $P(q)$. The first ideal step towards obtaining structural information is to determine the R_g using Guinier approximation according to the following equation [107].

$$\ln I(q) = \ln I(0) - R_g^2 q^2/3 \tag{13}$$

$I(0)$ represents the intensity of scattered light as zero angle. Since it is practically not possible to collect such information experimentally, a plot of $(I(q))$ vs. (q^2) is used to obtain $I(0)$. For globular macromolecules, the $R_g q$ range is from 0.7 to 1.3. Monodisperse sample preparation will result in a linear Guinier plot, whereas aggregation results into a nonlinear Guinier plot [105,108].

Alternatively, it is also possible to perform indirect Fourier transformation and convert the reciprocal-space information of $\ln(I(q))$ vs. (q) into real space distance distribution function $(P(r))$, that provides information on maximum particle dimension (D_{max}), R_g, and the shape of macromolecules (Glatter, 1977).

$$P(r) = \frac{r^2}{2\pi^2}\int_0^\infty q^2 I(q)\frac{\sin(qr)}{qr}dq \tag{14}$$

where, $P(r)$ represents the electron pair-distance distribution function and D_{max} is the maximum distance in the scattering macromolecule. In addition to providing information on D_{max} and R_g, the shape of the $P(r)$ plot reflects the gross solution conformation of the macromolecule, and is discussed further in review articles [102,109,110]. Compared to X-ray diffraction studies, where the macromolecules are arranged in a fixed position in a crystal lattice providing information on the directionality of atoms, in SAXS studies, the macromolecules are in a continuous motion, randomly oriented and positioned, resulting in scattering of X-rays that provides information on the average solution size of macromolecules. In addition to the determination of R_g and D_{max}, SAXS can also provide information on M_w estimates as discussed in [102,105,108].

SAXS also allows examination of folded/unfolded state of macromolecules based on the Kratky analysis method, where a plot of $I(q)q^2$ *vs.* q is constructed. For globular macromolecules the Kratky plot results in a bell-shaped distribution, whereas for extended or unfolded macromolecules, the $I(q)q^2$ increases with an increase in q, reaching a plateau [111]. However, the main concern with this method is that the y-axis values $(I(q)q^2)$ depend on the M_w and concentration of macromolecules, which makes it difficult in the case of comparison of macromolecules with different sizes. Further, this method may not be suitable to study partially folded macromolecules that contain certain folded regions. Therefore, a modified version, known as the *normalized* or *dimensionless* Kratky analysis was proposed [112,113]. In this method, the intensity $I(q)$ is normalized to $I(0)$, and q is normalized to R_g of macromolecules to plot $(qR_g^2)I(q)/I(0)$ *vs.* qR_g. The normalized method of Kratky plot offers two benefits. First, by dividing the $I(q)$ by $I(0)$ that depends on the M_w of macromolecules, the plot becomes independent of the M_w of macromolecules. Second, the multiplication of q with R_g gives angular scale that does not dependent on protein size, compared to the traditional Kratky plot. Ultimately, this method provides more reliable information on partially unfolded and disordered proteins as well as allows comparison of SAXS data for different macromolecules [108,114].

2.3.3.1. Benefits and limitations. SAXS offers many advantages compared to SEC, AUC, DLS, SEC-MALLS and other methods for characterization of macromolecules. For example, it is possible to determine M_w that does not depend on the shape of calibrant and of macromolecules under investigation, unlike SEC. SAXS data can distinguish monomer from dimer, and can perform simultaneous shape reconstruction using the program MIXTURE [115], unlike DLS. AUC provides information on the gross conformation of macromolecules (i.e. if the macromolecules are globular or extended); however, SAXS *ab initio* models can provide a significantly more detailed description of macromolecular shape. In addition, unlike AUC, where it is possible to find out (Yes/No answer) if conformational changes occur with a particular species, by application of SAXS, it is actually possible to visualize conformational changes that occur [116]. SEC-MALLS is limited to very large macromolecules or larger macromolecular assemblies in terms of determining R_g, and typically not very useful for individual proteins, nucleic acids or smaller complexes. SAXS can provide accurate information on R_g for macromolecules down to 1 nm. In addition, many synchrotron light sources now have HPLC-SAXS instrumentation, which can separate aggregates, degraded products or unbound macromolecules from the complex to provide reliable scattering information on a monodisperse fraction.

Although NMR, X-ray crystallography, and cryo-electron microscopy enable determination of structures at the atomic level, flexible regions in macromolecules, large size, and complexes involving multiple species are some of the challenges both methods encounter, preventing their application for a particular system. SAXS in such cases can be used as a complementary method where a portion of a complex or individual stably folded components can be studied with NMR/X-ray crystallography/cryo-electron microscopy to obtain high-resolution structure(s). On the other hand, the entire system can be studied using SAXS to obtain low-resolution shape information. Finally, both, high-resolution and low-resolution data can be combined using various data analysis tools (see Sections 2.4 and 2.5) to obtain a global picture that contains relative positions and orientations of macromolecules in complexes. Furthermore, a structure determined using X-ray crystallography might have crystal related artifacts, for example, an oligomeric arrangement that is enforced by crystal packing. SAXS can also be used to confirm the solution structure of a determined X-ray crystal structure [117]. Thus, to gain information on size and shape of macromolecules and their complexes, SAXS is a useful method that requires very small amount of sample (~15–50 μL, Table 1) and relatively small amount of experimental time.

SAXS provides an averaged information on macromolecules or their complex in solution, and therefore sample homogeneity is the single most important factor influencing the reliability of the data obtained. The danger with SAXS analysis is that the presence of high M_w aggregates could lead to a wrong structural interpretation, especially because the $I(0)$ is proportional to the M_w^2. Therefore, if the preparation is not monodispersed, misleading conclusions can be achieved. As the light scattering depends on the size of macromolecules, as low as 5% high M_w aggregates in samples can lead to overestimation of R_g and D_{max}. Prior to performing SAXS data collection, homogeneity checks using native gel electrophoresis, SEC, DLS, AUC-SV and/or SEC-MALLS must be performed. In the authors' laboratories, it is a standard practice to utilize multiple methods prior to data collection to ensure sample homogeneity and stability. Further, radiation damage of samples due to application of high-energy of X-rays should be checked by comparison of sample quality prior to and after SAXS data collection. Since SAXS is a contrast method, where the

scattering contributions from the solvent is subtracted before the data analysis, it is highly recommended that the solvent blank matches with the solvent that was used to solubilize macromolecules. In order to avoid interparticle interactions, SAXS data should be collected at multiple concentrations and the R_g values should be checked for each data set prior to merging the data. Often, SAXS data/models based on single concentration have been presented and far-reaching conclusions have been made: such practice should be avoided. As the light scattering also depends on the concentration of macromolecules in addition to the size, optimization of concentration range may be required for smaller macromolecules.

2.3.4. Small angle neutron scattering

Small angle neutron scattering (SANS) employs neutrons rather than the X-rays to study low-resolution shapes of macromolecules and their complexes. In combination with SAXS, SANS has emerged as a powerful technique to study RNA-protein complexes [118–121]. In contrast to SAXS, in SANS, a solution containing macromolecules is exposed to neutrons that interact with the nuclei of atoms. In X-ray scattering, the scattering length is proportional to the number of electrons (*i.e.* atomic number). Therefore, hydrogen (H), one of the most common elements in biological systems, has a very small scattering length (3.8×10^{-13} cm) resulting in poor scattering. In addition, elements such as carbon, nitrogen, and oxygen that are also commonly present in biological macromolecules have a highly similar scattering lengths for X-rays ($16.9–22.5 \times 10^{-13}$ cm). On the other hand, for neutrons, the scattering length for H is -3.74×10^{-13} cm. In case of deuterium (D), the scattering length for X-rays and neutrons is 2.28×10^{-13} cm and 6.67×10^{-13} cm respectively [122]. Thus, the major difference between the X-ray and neutron scattering for biological macromolecules is the negative value of the scattering length for H for neutron scattering, that allows neutrons to scatter, from hydrogen to 180° out of phase. Further, the difference between the scattering lengths of H and D in neutron scattering implies that the scattering from H_2O and D_2O will be different, unlike for X-rays, where scattering length for H and D is highly similar. Thus, neutron scattering offers benefit of matching the solvent background with the scattering from macromolecules, essentially providing a possibility to "hide" some component(s) of the macromolecular complex and visualize only selected one(s) by adjusting the ratio of H_2O:D_2O mixture (contrast variation method, [123]). Therefore, for a biomolecular complex composed of protein-nucleic acids or protein-carbohydrates, neutron scattering can be a highly useful method since the differences in scattering densities between proteins, nucleic acids, and carbohydrates, due to the differences in their atomic compositions can be taken advantage of, by mixing H_2O-D_2O at different ration to mask scattering contribution from one of the two interacting partners. The relationship between neutron scattering length for proteins and nucleic acids in H_2O and D_2O is discussed in more detail elsewhere [124]. SANS data are processed similarly to the SAXS data. SANS is often being employed as a complementary technique with other structural biology techniques, NMR, and computational modeling [125–127].

2.3.4.1. Benefits and limitations. As the H_2O:D_2O ratio is adjusted to allow visualization of one type of macromolecules and mask contributions from others, it is possible to investigate conformational changes that occur by interaction of the binding partner. SANS also allows application of wider range of buffer components (*e.g.* high salt buffers) relative to SAXS. SANS is a gentle technique compared to SAXS, resulting in significantly less radiation damage of macromolecules. However, neutron scattering offers relatively low flux compared to X-ray scattering, requiring higher concentrations of samples for data collection. Moreover, neutron sources are highly expensive, limiting their availability as compared to the SAXS.

2.4. Computational modeling of proteins, RNAs, and their complexes, with restraints from experimental data

2.4.1. Classification of macromolecular modeling methods

There exist a wide variety of methods for macromolecular 3D structure prediction that are applicable to nucleic acids, proteins, and their complexes. They can be classified in various ways. One classification divides structure modeling methods into those based on the fundamental laws of physics that govern the process of folding (i.e. the "Greek science" approach), and all others, which typically extensively use information about other structures, available in various databases (i.e. the "Babylonian science" approach) [128,129]. A number of computational methods based on either of these approaches may perform model building with the use of restraints derived from biochemical or biophysical experiments (i.e. to bias the modeling process to fit the experimental data) [130–133].

Modeling based on fundamental laws of physics is accurate but very slow. The function with which to calculate the energy should be ideally based on quantum-mechanical (QM) description of the system. However, such calculations are extremely complex, therefore they are applicable only to very small molecules. Therefore, various simplifications are used and typically the system is described in terms of Newtonian dynamics (*e.g.*, as in Molecular Dynamics methods), but even then, physics-based methods can only be used to model relatively small macromolecules. An alternative approach is to limit the conformational space by user-defined restraints. For instance, solution scattering data can be used as a differentiable energetic restraint in explicit-solvent MD simulations, with the aim to direct the simulation into conformations satisfying the experimental data [134]. Molecular dynamics simulations initiated with experimentally determined structures and heavily restrained by experimental data have been used to model the conformational transitions of RNA-containing macromolecular complexes as large as entire ribosome [135].

The modeling can be made much faster by further simplifications. Full-atomic resolution models represented in Cartesian coordinates utilize three degrees of freedom (x, y, z) for each atom, therefore even for small molecules, the conformational space is enormous, which is challenging in terms of computational requirements to perform a simulation of macromolecular folding or binding. One way to reduce the number of degrees of freedom is to restrict bond lengths and/or angles to idealized values to reduce approximately 10-fold the number of adjustable parameters that characterize a model. Further simplification can be achieved by coarse-graining, in which groups of atoms may be treated as single interaction centers or "pseudoatoms", so that a smaller number of elements and interactions is considered [136,137]. The simplification can span different levels of detail – from several interaction centers per amino acid or nucleotide residue to a single pseudoatom per element of secondary structure; such approach has been used, *e.g.* for the refinement of low-resolution structures of ribosomal RNAs with restraints from experimental data [138].

The accumulation of experimentally determined structures of proteins, RNAs, and their complexes has enabled the development of methods for macromolecular structure prediction that are not based on first principles, but extensively use the knowledge of "what the structures should look like". One type of the knowledge-based "Babylonian science" approach exploits databases to derive statistical potentials for macromolecular simulations and for scoring of models. The so-called mean force potentials, compiled by using the Boltzmann's principle, can take into account all forces acting between atoms of the molecule under

study as well as the influence of the environment, without the need of defining each type of interactions separately [139]. It is also possible to use existing molecular structures in a different way: instead of modeling the physical process of macromolecular structure formation, one can predict how do the macromolecular structure changes in the course of the evolution. This type of structure prediction relies on empirical observation that evolutionarily related (homologous) macromolecules usually retain the three-dimensional structure despite the accumulation of divergent mutations [128,140]. Therefore, experimentally determined structures can be used as "templates" to model structures of macromolecules that are expected to be related by homology. This approach is usually referred to as "comparative modeling", "homology modeling", or "template-based modeling". A third knowledge-based strategy is intermediate between the two mentioned above: it involves the assembly of macromolecular structures from fragments that may be taken from experimentally determined structures or predicted computationally with any approach. The scoring functions used can utilize physical or statistical potentials or the combinations of both, and they often enable the use of experimental data from various sources.

2.4.1.1. Benefits and limitations. Physics-based methods for macromolecular structure modeling can often yield accurate and reliable models for relatively small molecules. However, it is still not feasible to predict, with the use of pure theory, structures of large macromolecules, unless they have related structures in the database. On the other hand, the use of the knowledge-based approach is limited only to target macromolecules for which a structurally similar template exists in the database, but this target-template relationship must be correctly identified. This limitation can be partially overcome by incorporation of experimental restraints, which can be used either explicitly in the modeling process or for scoring and ranking of alternative models obtained.

One of the problems that plagues computational structure prediction according to the physics-based approach is the large number of local minima of the scoring function that need to be sampled, and as a result – a large number of alternative conformations that have to be analyzed. Force fields derived for coarse-grained systems typically yield a much smoother energy surface than those used for all-atom systems. As a result, many local minima are removed, thus reducing the probability that a macromolecule is trapped in a suboptimal energy state during the simulation. However, it must be emphasized that simplifications of the model representation and the energy function enhance the modeling speed usually at the cost of accuracy of the structures obtained. Thus, it is not practical to expect that a folding simulation with a coarse-grained representation would confidently predict a native-like protein or RNA structure with a precisely estimated energy. On the other hand, the use of such simplified methods may be the only practical way to computationally fold a structure that is too complex for methods utilizing a full-atom representation and a physical potential that is more expensive to calculate.

The two problems of sampling and scoring can be addressed by using different modeling methods, different representations and different precisions and weights of structural restraints during different stages of the modeling. For instance, the initial modeling may be done with template-based "Babylonian science" methods that can approximate the target structure based on the laws of evolution, which allow to avoid extensive sampling. Alternatively, coarse-grained methods can be used to generate a large number of models that approximately satisfy the imposed restraints. Then, these models can be scored and/or clustered, to find groups of alternative solutions that appear reasonable and can be used as starting structures for the next stage of the modeling procedure, with increased resolution of the representation and with more precise restraints. For modeling of RNA-protein complexes, this usually means that structural models of individual components should be generated first by methods that are dedicated to either protein or RNA 3D structure prediction. As a second step, computational RNA-protein docking is performed, usually with structures of individual components (or at least one of them) modeled as rigid bodies, and with restraints on RNA-protein interactions obtained from various sources. Third, details of the complex structures are optimized. At all stages of modeling, one must be careful to avoid overfitting, especially with the use of restraints derived from low-resolution experiments that should not be over-interpreted.

2.4.2. The use of experimental data to guide macromolecular structure prediction

The restraints can describe various structural parameters of a macromolecule, such as local conformation (secondary structure), solvent accessibility, interatomic distances (*e.g.* tertiary contacts), detailed structures of individual components, or a 3D shape of the entire molecule. In each of these categories restraints can be obtained based on the results of various biophysical and biochemical experiments, and in many cases, they can be also predicted from additional computational analyses, or both. Here we focus specifically on the use of solution scattering methods reviewed earlier in this article, while for the use of other types of methods we refer the readers to other specialized reviews on approaches developed for protein structures [137] and nucleic acids structures [131,141–143].

Restraints on the shape of protein and RNA macromolecules and their complexes can be obtained from small angle scattering (SAS) experiments that utilize either X-ray (SAXS) or neutron (SANS) radiation. SAS data can be used for ranking the model structures obtained by large-scale computational simulations (*e.g.*, from RNA-protein docking experiments) to identify structures that best explain the observed data using, for example, the FOXS server [144]. The prediction of scattering curves with explicit solvent Molecular Dynamics simulations can be used to take into account the hydration layer and the excluded solvent, thereby avoiding any solvent-related fitting parameters, while naturally accounting for thermal fluctuations (*e.g.*, as implemented in the WAXSiS server [145]). Although the calculation of theoretical scattering curves is computationally expensive, it can be vastly reduced by employing proper representation of the atomic model like spherical harmonics or Zernike polynomials expansion (as implemented in CRYSOL [146] and SASTBX [147] respectively). The availability of fast methods for estimating SAS curves from atomic models also enables studies of conformationally heterogeneous structures. If a single model cannot explain experimental data, tools like Minimal Ensemble Search [148] or Ensemble Optimization Method [149,150] can be used to identify a small set of most probable components from a pool of states generated with bioinformatics modeling tools (see Sections 2.5.2 and 2.5.5). SAS data can also be used to obtain "*ab initio*" shape reconstructions at low-resolution, with several computational methods available for this purpose, *e.g.* DAMMIN/F [151,152]. Various modeling programs can be then used to perform fitting of pre-modeled protein and RNA 3D structures into these shapes, and best-fitting structures may be selected as the most promising models, *e.g.* as it was done for the determination of a structure of T-box RNA complexed with tRNA [153].

The global shape of large RNA-protein complexes can also be directly observed using the electron microscopy done in cryogenic conditions (cryo-electron microscopy). The recent advancements in instrumentation has allowed investigation of molecules that are ~100 kDa with a resolution of ~2.3 Å [154,155]. The three-dimensional structure reconstruction is done based on a large number of collected two-dimensional projections. Cryo-electron

microscopy has been instrumental for the modeling of RNA structures in the context of many important RNA-protein complexes, *e.g.* Ribosome [156], spliceosome [157,158], or cascade complex [159].

2.5. Modeling software

2.5.1. Software for modeling of individual protein and RNA 3D structures

Computational modeling of protein structures is a mature field, and a large number of prediction methods exist, whose development has been fueled by a large amount of experimental data from structural genomics projects. On the other hand, there are much fewer structures of RNA, and consequently, fewer modeling methods. The accuracy of individual programs and prediction approaches have been compared in community-wide experiments: Critical Assessment of methods of protein Structure Prediction (CASP; *e.g.*, [160] and references therein) and RNA Puzzles [161,162].

A subjective short list of methods that perform well according to benchmarks, are relatively easy to use (often are available both as a standalone method and as a web server), and have been often used in the context of RNA-protein complex modeling by the authors of this article, include: MODELLER [163,164] and SWISS-MODEL [165,166] for template-based modeling of protein structures, CABS [167,168], ROSETTA [169,170], and I-TASSER [171,172] for template-free and hybrid modeling of protein structures, ModeRNA [173,174] for template-based modeling of RNA structures, and FARNA [175] and SimRNA [176,177] for template-free and hybrid modeling of RNA structures. Supplementary Tables 1 and 2 provide a list of packages for protein and RNA structure prediction respectively, with a brief description and web link for each package.

2.5.2. Software for 3D shape modeling based on SAS data

Small angle scattering is a low-information content technique. The actual number of independent observations depends on the data quality, maximum resolution, shape and size of the studied particles. Theoretical analysis of the SAS curve information content for an idealized experimental setup suggests that the number of independent observations recorded for biological samples is in the order of few tens [178]. A more accurate estimate for a specific case that takes into account data quality can be obtained using recently developed SHANUM program from the ATSAS suite [179]. Nevertheless, one should always bear in mind that there is a large danger of overfitting in the macromolecular modeling based on SAS data. Therefore, the number of parameters of a model should be reduced as much as possible. In the case of RNA-protein complexes an optimal strategy is to perform rigid-body docking of components obtained independently from other sources (see Section 2.5.3).

The earliest study involving *ab initio* model reconstruction for lysozyme was performed in 1998 by Chacon et al. [180]. After a decade, the same approaches were applied to obtain low-resolution shape information on nucleic acids [181–183]. The modern approaches to build low-resolution *ab initio* models based on simulated annealing methods with preliminary information on R_g and D_{max} using programs DAMMIN [152], DAMMIF [151] and GASBOR [184] are discussed by [100,102] and have been extensively utilized by our group [1,5,6,8,51,116,185–188]. Furthermore, SAXS data can be used to combine high-resolution structure information for individual domains to fit in a full-length or a chimeric protein or to study protein-protein/protein-nucleic acid interactions by performing rigid-body analysis using programs BUNCH [189], CORAL [190], SASREF [189], FoXS family packages [191] and SAXSTER [238]. Application of SAXS data for rigid-body modeling is rapidly growing in application [5,18,52,192–200]. A list of computational packages for high-resolution modeling of macromolecules based on SAXS data is outlined in a recent review by Trewhella [103]. We have also provided an updated list of packages with their web link in the Supplementary Table 3. Recently, review articles describing RNA 3D modeling using SAXS as a complementary tool [201–203], SAXS analysis of RNA-protein and RNA-RNA complexes [204,205] and application of NMR in combination with SAXS data to study the structures of macromolecular assemblies [206–208] have been published. In addition, readers are also advised to refer to other excellent review articles for details on theories and applications of SAXS [60,62,100,102,104–106,109,110].

2.5.3. Software for modeling of RNA-protein complex structures with the use of experimental data

With atomic models of protein and RNA components one can proceed with the docking of the two structures in order to build a complete model of the complex [209,210]. In general, two approaches are available. One is to generate a large pool of plausible complex models with docking tools that enable RNA-protein docking like NPDock [211], PatchDock [212], or HADDOCK [213] and score them against experimental SAXS data using *e.g.* FOXS [144] or CRYSOL [146]. Another possibility is to build complex models with tools that can directly use SAS data to restrain docking process. Currently available programs that can be used for that purpose include IMP [144], pyDockSAXS [214], and FoXSDock [191] and PyRy3D (developed in the Bujnicki laboratory and available at http://genesilico.pl/pyry3d). It is worth mentioning that FoXSDock is the only SAXS-based docking method that additionally provides multi-state scoring function. It enables modeling of complexes when a sample contains a mixture of monomers and the complex. Such an approach, however, must be used with care and one should ensure homogeneity of the sample with the biochemical methods discussed above.

An important issue with the above-mentioned docking methods is the assumption that complex components conformations are similar in their free and bound states. Although *e.g.* HADDOCK allows for a limited flexibility of docked macromolecules at the predicted interface it will not allow for larger conformational changes. In the context of SAS-restrained modeling, it helps to avoid overfitting but may make building complexes involving large and flexible RNAs very difficult. For this reason, we have developed a new protocol for modeling RNA-protein complexes that exploits modular architecture of RNA. In this approach, individual helices of RNA (together with hairpin loops at their ends) were modeled as rigid bodies, restrained at the junction to maintain the continuity of the nucleotide chain. Such a "marionette" model of RNA can be modeled together with the protein component (potentially also divided into small parts) to build a complex that agrees with experimental data restraints. (Fig. 2) [6]. Initially, we used this modeling strategy for docking, with the use of PyRy3D, the model components into low-resolution *ab initio* reconstructions of the complex shape (obtained *e.g.* with DAMMIN program, Fig. 2 panels 3 and 4). With the recent versions of PyRy3D, however, one can use SAS curve to directly restrain the docking simulation, which is highly recommended. With that approach, the final atomic model can be compared with independently obtained low-resolution shape reconstruction providing an additional quality check of the results. Moreover, the simulation process is much easier to initiate making it less error-prone and more accessible for non-specialists.

2.5.4. Software for validation of 3D structure models against SAS data

FoXS (Fast X-ray Scattering) is a web server available with an intuitive interface at http://modbase.compbio.ucsf.edu/foxs/index.html. It is used for rapidly computing a SAXS profile of a given molecular structure and its fit with experimental SAXS profiles if

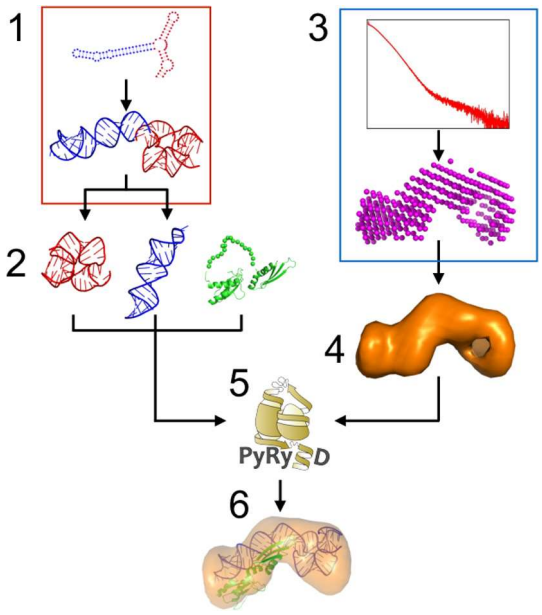

Fig. 2. Outline of the semi-flexible modeling of RNA-protein complexes with PyRy3D. (1,2) Input model preparation. The structural models of complex components can be obtained from databases of experimentally-determined structures (in particular from the PDB) or modeled by computational methods. (3,4) Determination of *ab initio* shape reconstruction from SAS data and calculation of pseudo-EM density map. (5) Restrained docking of the individual components to the low-resolution map. (6) Geometry refinement of the final model.

provided [144]. The algorithm to compute SAXS profile is based on the Debye formula. As an input, it takes a mandatory one structure file in the PDB format (or a zip archive with multiple PDB files) to compute its SAXS profile. The optional input includes an experimental SAXS profile (as .dat file). Computing SAXS profile of a molecular structure and its fitting with SAXS experimental profile is performed rapidly in real time. The output page displays a plot of the computed profile as well as a plot of the computed profile fitted to the experimental profile. In addition, the values of fit parameters (χ, excluded volume, hydration layer density) and R_g for the current profile are displayed. Closer the value of χ to 1, better the molecular structure fits the experimental SAXS profile.

CRYSOL calculates solution scattering profile from the macromolecular structure and fits it with the experimental SAXS profile [146]. The software can be downloaded as an ATSAS package from https://www.embl-hamburg.de/biosaxs/download.html. Alternatively, CRYSOL web server can be accessed from https://www.embl-hamburg.de/biosaxs/atsas-online/crysol.php. As an input, one can use a structure of a protein or a protein-DNA(RNA) complex (in PDB format) and an optional experimental SAXS profile (as .dat file). CRYSOL uses multipole expansion of the scattering amplitudes to calculate the spherically averaged scattering pattern and takes into account the hydration shell. If the SAXS experimental data is provided, CRYSOL can fit the theoretical scattering curve by minimizing the discrepancy (χ^2 value). Supplementary Table 3 presents a list of data analysis packages that can be used to validate high-resolution structures against solution scattering data.

2.5.5. Software to study disordered and flexible systems

In a biological system, there are many cases where the RNA, protein and/or their complexes are flexible in nature. Conversely, the protein of interest may be disordered in solution. Significant progress has been made over the last few years to study disordered and flexible systems. For example, the shape reconstruction based on SAXS data of disordered and flexible macromolecules can be performed by means of Ensemble Optimization Method [149,215] and ENSEMBLE program [216]. The BILBOMB minimal ensemble search algorithm combines the SAXS data analysis for disordered and flexible system with molecular dynamics calculations [114,148]. On the other hand, the Basis-Set Supported SAXS algorithm SAXS data analysis with coarse-grained analysis can also be employed [217]. Furthermore, the Bayesian ensemble SAXS package [218] and Ensemble Refinement of SAXS package [219] can also be used to obtain structural information on flexible and disordered systems. In addition, the programs such as MONTEHYDRO [220] and SIMUFLEX [221] can be used to calculate hydrodynamic parameters and scattering intensities from disordered and flexible macromolecules and their complexes [222].

2.5.6. Application of hydrodynamic properties for model validation

Apart from the application of hydrodynamic methods to study homogeneity, conformational changes and in some cases M_w, these methods also provide useful parameters such as s, R_h, R_g and D_{max} for RNA, proteins, and their complexes. In addition to the standard crosschecks, each modeling method utilizes, hydrodynamic parameters could be used to independently validate low- and high-resolution models by comparing experimentally determined and model derived parameters. The HYDRO-family packages [223,224] and UltraScan Solution Modeler (US-SOMO) [225,226] are widely used to calculate such hydrodynamic properties from low- and high-resolution structures. Typically, the input parameters require structure coordinates file (PDB format), the molecular weight of samples, density and viscosity of buffer and experimental temperature. The detailed description of the hydrodynamic modeling and the approaches these programs employ to provide information on hydrodynamic parameters are discussed elsewhere [227–229]. However, their brief description and web links are presented in Supplementary Table 4. We have used such approaches to derive hydrodynamic properties from models calculated using solution scattering data and computational modeling approaches to validate RNA, protein as well as RNA-protein complexes to independently validate the hybrid models [1,5,6,8,23,51,52,116,185,187,230].

3. Case studies

3.1. Pentatricopeptide repeat protein (PPR10) – RNA complex

The pentatricopeptide repeat (PPR) proteins belong to an alpha-solenoid superfamily, that are found to be present in all eukaryotes and plants, and are composed of 2–30 tandem repeats of degenerate 35 amino acids. The PPR family proteins play vital roles in RNA editing, maturation, post-transcriptional modifications and stabilization in mitochondria and chloroplast [231–236]. The interaction studies of recombinant PPR10 protein (chloroplast pentatricopeptide repeat protein 10, residues 69–786, 82.5 kDa) from Maize (*Zea Maize*) with 17-nucleotide (nt) (*atpH*) and 18-nt (*psaJ*) RNA oligonucleotides illustrates the methodologies discussed in previous sections. PPR10 expressed in *E. coli* was partially purified using its MBP fusion tag, cleaved, and purified using SEC [237]. Previous studies suggested that PPR10 self-associates readily [238], and therefore SEC-purified PPR10 was studied by AUC-SV. A monomer-dimer equilibrium was observed, with a monomer peak (~5S) gradually decreasing in area relative to a dimer (6.5S) as PPR10 concentration was increased. Complex formation with an equimolar concentration of 17-nt RNA (~5 kDa) presented single peak at 4.9S, suggesting that the presence of RNA is sufficient to prevent dimer formation [237]. SEC-purified PPR10 with mutations designed to prevent disulfide formation (residues 69-786, C256S/C279S/C430S/C449S) was subsequently crystallized alone or in

complex with the 18-nt *pasJ-RPL33* intergenic region [239]. The crystal structure of PPR10 revealed that although there is only one molecule of PPR10 present in the asymmetric unit, two symmetry-related macromolecules were present in an antiparallel orientation. The antiparallel dimer of PPR10 was observed in complex with *psaJ*. However, the PPR10 undergoes a conformational change where the N- and C-terminal helices are located towards the center of the structure resulting in decrease in axial length of PPR10 by 20 Å. Attempts to crystallize a second PPR10 complex with the *atpH* RNA were not successful, but AUC-SE experiments demonstrated that *atpH* and not *psaJ* was able to weaken dimerization of PPR10 [239]. A third study used HPLC-SAXS experiments to obtain solution structure of PPR10-*atpH* (87.8 kDa) at lower concentrations [240]. Using PPR10 and *atpH* high-resolution structures with SAXS data for the complex as a constraint, the PPR10-*atpH* complex was found to be monomeric in solution, as evidenced by the AUC-SV studies [237]. Therefore, the integrated use of SEC, AUC-SV, AUC-SE, SAXS, and modeling suggest differences in both affinities and dimerization of PPR10 with *psaJ* and *atpH*.

3.2. Interaction between tRNA-modifying enzymes (MnmE/MnmG) with GTP

In bacteria, MnmE and MnmG form a complex (MnmE/MnmG) responsible for the carboxymethylaminomethyl modification of uridine 34 of tRNA. MnmE contains an N-terminal α-helical domain (enabling dimerization), and a C-terminal G domain that toggles between a GDP bound "open state" and a GTP-dependent "closed state" where interaction of G-domains enables rapid GTP hydrolysis [241–243]. Based on SEC-MALLS and with SAXS *ab initio* modeling [87], MnmE alone is a dimer with the G domains not interacting, while MnmE in the presence of GDP-AlFx is consistent with the open state based on a homology model of MnmE [241] with the G-domains interacting that could back-calculate SAXS scattering data. MnmG is composed of an N-terminal FAD-binding domain and a C-terminal helical domain, and forms a stable dimer by SEC [244]. HPLC-SAXS studies of *A. aeolicus* MnmG displayed self-association at high concentrations and *ab initio* structures that agreed well with the dimeric high-resolution structure [87]. SEC-MALLS studies confirmed a dimer of MnmG.

3.2.1. Only one of the two MnmG interacts with $tRNA^{Lys}$ in solution

SEC-MALLS studies of the MnmG-$tRNA^{Lys}$ complex yielded a M_w consistent with one tRNA molecule bound to the MnmG dimer. *Ab initio* shape reconstructions of the complex using HPLC-SAXS confirmed that only one of the MnmG domains shows presence of extra volume [87] relative to MnmG alone, and docked models of the predicted complex (PatchDock [212]) were consistent with SAXS data (using CRYSOL [146], as discussed in Section 2.5.4) [87]. The docked model had the anticodon stem-loop of the tRNA (where uridine 34 is located) localized in the FAD-binding pocket of MnmG and near two catalytic residues.

3.2.2. Dimeric MnmE/MnmG complex

SEC-MALLS analysis of the MnmE-MnmG complex suggested a dimer of dimers, with an L-shaped assembly predicted by HPLC-SAXS. Docked complexes were then scored based on agreement with SAXS data (using CRYSOL [146]), alignment with the *ab initio* models, proximity of active sites and vacancy of the tRNA binding site on MnmG [87]. This analysis suggested that the C-terminal domain of an MnmG monomer interacts with the N-terminal domains of the MnmE dimer, such that the cofactor-binding sites of MnmE/MnmG are oriented towards each other allowing tRNA modification by MnmG [87].

3.3. Recognition of the West Nile Virus (WNV) genome by 2′- 5′-oligoadenylate synthetase 1 (OAS1)

The interaction between human OAS1 and the double-stranded RNA (dsRNA) terminal regions (TR) of the WNV genome was investigated using a combination of DLS, AUC-SV, SAXS, and computational modeling [8,51]. OAS1 is a dsRNA-activated enzyme that is central to the innate immune response to WNV infection, and these studies sought to determine the recognition site on the viral genome. The individual 5′- and 3′-terminal regions of the WNV genome (5′-TR and 3′-TR) were investigated because of their dsRNA character and that they undergo unfolding and the establishment of new long-range base-pairing interactions between the TR during viral replication [245]. SEC-purified OAS1 exhibited a single peak by AUC-SV and DLS measurements, consistent with both the predicted M_w and *ab initio* models generated by SAXS [51]. The high-resolution structure of human OAS1 superimposed well with the *ab initio* models as well [246].

Based on RNase probing experiments, the 5′-TR of the WNV genome adopts three distinct dsRNA stem-loops [247]. DLS of the 5′-TR suggested suitability for SAXS analysis, and interestingly two closely-related conformations of the 5′-TR were observed in *ab initio* SAXS reconstructions suggesting flexibility of the molecule in solution [51]. One of the conformations corresponds to the expected secondary structure, the other lacks definition potentially capturing a partially unfolded conformation. OAS1 binding does not significantly perturb the solution structure of the 5′-TR as determined by SAXS, but instead presents a disc-shaped protrusion from the RNA, consistent with the human OAS1 structure. Binding/enzymatic studies confirmed the requirements of specific stem-loops in the 5′-TR for OAS1 interaction.

The 3′-TR studied by SAXS adopts an extended dsRNA conformation in solution, and was cross-validated by DLS. Computational models using the SAXS data and RNA secondary structural data as

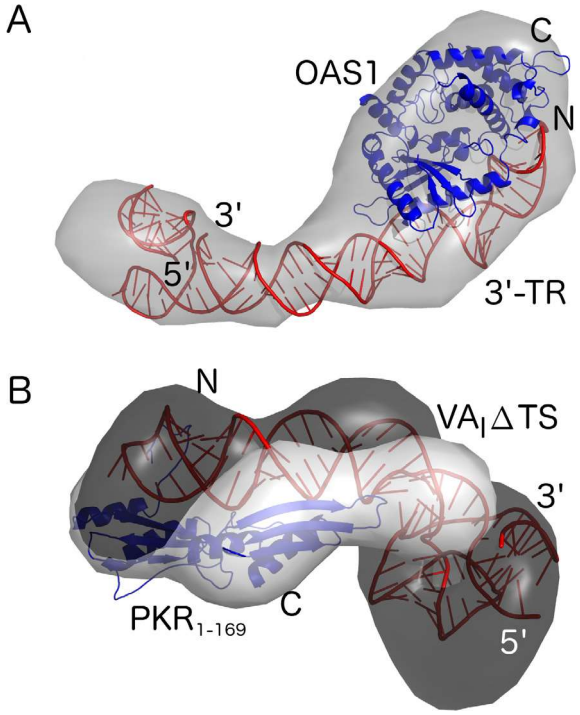

Fig. 3. Computational modeling of protein-RNA complexes with the use of Small Angle Scattering data. (A) Atomic model of human OAS1 and 3′-terminal regions of the WNV with the corresponding ad-initio reconstruction. (B) Atomic model of the RNA binding domains of PKR and VAIΔTS built based on the *ab initio* reconstructions of protein (light gray) and RNA (dark gray) components of the complex.

restraints (using SimRNA/PyRy3D modeling pipeline) suggested a bent and extended A-RNA helical structure with the bottom of a long and short-stem loop stacking on each other. OAS1-3′-TR complex formation studied by SAXS and computational modeling of the existing 3D structure of OAS1 was consistent with biochemical data demonstrating interaction with the long stem loop, and does not significantly perturb the RNA structure (Fig. 3). The experimentally determined structure of OAS1 [246] and refined model of the 3′-TR RNA were treated as rigid bodies and additional restraints were used to keep OAS1 residues involved in protein-RNA interactions close to the RNA chain.

3.4. Solution conformation of adenovirus associated RNA-I (VA_I)

During the late stages of adenovirus infection, VA_I RNA (~160 nt) accumulates to high concentration to help enable efficient translation of viral mRNA in part by inhibition of the RNA-dependent protein kinase (PKR) [248–250]. VA_I consists of dsRNA with an apical stem-loop (AS), a central stem-loop, (CS), and a terminal stem (TS) meeting at a three-way junction (3wj) [251]. Using a combination of DLS, AUC-SV, SAXS, and computational modeling, the solution structure of VA_I and its interaction with a protein binding partner (RNA-dependent protein kinase, PKR) was determined [6]. VA_I preparations were monodisperse, with DLS, AUC-SV, and SAXS analysis yielding results consistent with an extended RNA structure. SAXS analysis of $VA_I\Delta TS$ revealed a $P(r)$ distribution plot with a skewed bell shape at short radii with an extended tail suggesting an elongated RNA, and this was confirmed by *ab initio* solution structures and DLS measurements. Complex formation between the tandem RNA binding domains of PKR (dsRBMs; residues 1–169) and dsRNA stem-loops, including $VA_I\Delta TS$, have been studied using similar approaches [6,116]. SAXS analysis of $VA_I\Delta TS$ and dsRBMs alone enabled deconvolution of the *ab initio* model of the complex formed between them. Computational approaches were then used to predict the tertiary structure of the complex. The existing high-resolution structure of the dsRBMs [252], SimRNA-predicted $VA_I\Delta TS$ structure, known regions of flexibility in the protein, and the SAXS *ab initio reconstructions* were used in rigid-body modeling of the complex using PyRy3D (Fig. 3). Both dsRBMs mediated the interaction with the AS, with the first dsRBM interacting with the loop of the AS and the second dsRBM contacting the AS at is base near the 3wj. The high-resolution models also demonstrated that the CS of VA_I does not participate in interaction with dsRBMs [6].

Acknowledgements

We thank Krzysztof Skowronek for critical reading of the manuscript and useful comments. T.R.P. was supported by the University of Lethbridge Start-up fund. J.M.B. and A. were supported by the Polish National Science Centre (grant 2012/04/A/NZ2/00455 to J. M.B.). J.M.B. was additionally supported by the European Research Council (grant RNA+P=123D to J.M.B.) and by the "Ideas for Poland" fellowship from the Foundation for Polish Science (FNP). S.A.M. was supported by a Discovery Grant from the Natural Sciences and Engineering Research Council of Canada (RGPIN-2015-06142) and the Cancer Research Society.

Appendix A. Supplementary data

Supplementary data associated with this article can be found, in the online version, at http://dx.doi.org/10.1016/j.ymeth.2016.12.002.

References

[1] M. Meier, T.R. Patel, E.P. Booy, O. Marushchak, N. Okun, S. Deo, R. Howard, K. McEleney, S.E. Harding, J. Stetefeld, S.A. McKenna, Binding of G-quadruplexes to the N-terminal recognition domain of the RNA helicase associated with AU-rich element (RHAU), J. Biol. Chem. 288 (49) (2013) 35014–35027.
[2] J. VanOudenhove, E. Anderson, S. Krueger, J.L. Cole, Analysis of PKR structure by small-angle scattering, J. Mol. Biol. 387 (4) (2009) 910–920.
[3] R. Reeves, HMGA proteins: flexibility finds a nuclear niche?, Biochem Cell Biol. 81 (3) (2003) 185–195.
[4] R.P. Rambo, J.A. Tainer, Improving small-angle X-ray scattering data for structural analyses of the RNA world, RNA 16 (3) (2010) 638–646.
[5] T.R. Patel, G.A. Morris, D. Zwolanek, D.R. Keene, J. Li, S.E. Harding, M. Koch, J. Stetefeld, Nano-structure of the laminin gamma-1 short arm reveals an extended and curved multidomain assembly, Matrix Biol. 29 (7) (2010) 565–572.
[6] E. Dzananovic, T.R. Patel, G. Chojnowski, M.J. Boniecki, S. Deo, K. McEleney, S. E. Harding, J.M. Bujnicki, S.A. McKenna, Solution conformation of adenovirus virus associated RNA-I and its interaction with PKR, J. Struct. Biol. 185 (1) (2014) 48–57.
[7] T.R. Patel, C. Bernards, M. Meier, K. McEleney, D.J. Winzor, M. Koch, J. Stetefeld, Structural elucidation of full-length nidogen and the laminin-nidogen complex in solution, Matrix Biol. 33 (2014) 60–67.
[8] S. Deo, T.R. Patel, G. Chojnowski, A. Koul, E. Dzananovic, K. McEleney, J.M. Bujnicki, S.A. McKenna, Characterization of the termini of the West Nile virus genome and their interactions with the small isoform of the 2′ 5′-oligoadenylate synthetase family, J. Struct. Biol. 190 (2) (2015) 236–249.
[9] P. Andrews, Estimation of the molecular weights of proteins by Sephadex gel-filtration, Biochem. J. 91 (2) (1964) 222–233.
[10] P. Andrews, The gel-filtration behaviour of proteins related to their molecular weights over a wide range, Biochem. J. 96 (3) (1965) 595–606.
[11] T.R. Patel, D.J. Winzor, Reassessment of the size of the supermolecular state of Dishevelled-3, J. Mol. Recognit. 24 (5) (2011) 843–846.
[12] T.R. Patel, D.J. Winzor, The macromolecular state of A-kinase anchoring protein, J. Mol. Recognit. 25 (1) (2012) 11–14.
[13] T.C. Laurent, J. Killander, Theory of gel filtration + its experimental verification, J. Chromatogr. 14 (3) (1964) 317.
[14] G.K. Ackers, A new calibration procedure for gel filtration columns, J. Biol. Chem. 242 (13) (1967). 3237.
[15] I. Kim, S.A. McKenna, E. Viani Puglisi, J.D. Puglisi, Rapid purification of RNAs using fast performance liquid chromatography (FPLC), RNA 13 (2) (2007) 289–294.
[16] J. Stetefeld, S.A. MaKenna, T.R. Patel, Dynamic light scattering: a practical guide and applications in biomedical sciences, Biophys. Rev. (2016) 1–19.
[17] T.R. Patel, D.J. Winzor, D.J. Scott, Analytical ultracentrifugation: a versatile tool for the characterisation of macromolecular complexes in solution, Methods 95 (2016) 55–61.
[18] T.J. Green, S. Macpherson, S. Qiu, J. Lebowitz, G.W. Wertz, M. Luo, Study of the assembly of vesicular stomatitis virus N protein: role of the P protein, J. Virol. 74 (20) (2000) 9515–9524.
[19] S.J. Greive, A.F. Lins, P.H. von Hippel, Assembly of an RNA-protein complex. Binding of NusB and NusE (S10) proteins to boxA RNA nucleates the formation of the antitermination complex involved in controlling rRNA transcription in Escherichia coli, J. Biol. Chem. 280 (43) (2005) 36397–36408.
[20] M. Teplova, L. Malinina, J.C. Darnell, J. Song, M. Lu, R. Abagyan, K. Musunuru, A. Teplov, S.K. Burley, R.B. Darnell, D.J. Patel, Protein-RNA and protein-protein recognition by dual KH1/2 domains of the neuronal splicing factor Nova-1, Structure 19 (7) (2011) 930–944.
[21] C.J. Wong, K. Launer-Felty, J.L. Cole, Analysis of PKR-RNA interactions by sedimentation velocity, Methods Enzymol. 488 (2011) 59–79.
[22] M.J. Urban, I.T. Holder, M. Schmid, V. Fernandez Espin, J. Garcia de la Torre, J.S. Hartig, H. Colfen, Shape analysis of DNA-Au hybrid particles by analytical ultracentrifugation, ACS Nano (2016).
[23] R. Reuten, T.R. Patel, M. McDougall, N. Rama, D. Nikodemus, B. Gibert, J.-G. Delcros, C. Prein, M. Meier, S. Metzger, Z. Zhou, J. Kaltenberg, K.K. McKee, T. Bald, T. Tüting, P. Zigrino, V. Djonov, W. Bloch, H. Clausen-Schaumann, E. Poschl, P.D. Yurchenco, M. Ehrbar, P. Mehlen, J. Stetefeld, M. Koch, Structural decoding of netrin-4 reveals a regulatory function towards mature basement membranes, Nat. Commun. 7 (2016) 13515.
[24] T. Svedberg, K.O. Pedersen, The Ultracentrifuge, Oxford University Press, Oxford, 1940.
[25] S.E. Harding, Determination of absolute molecular weights using sedimentation equilibrium analytical ultracentrifugation, in: C. Jones, B. Mulloy, A. Thomas (Eds.), Methods in Molecular Biology, Humana Press, New Jercy, 1994, pp. 75–84.
[26] J. Lebowitz, M.S. Lewis, P. Schuck, Modern analytical ultracentrifugation in protein science: a tutorial review, Protein Sci. 11 (9) (2002) 2067–2079.
[27] T.M. Schuster, J.M. Toedt, New revolutions in the evolution of analytical ultracentrifugation, Curr. Opin. Struct. Biol. 6 (5) (1996) 650–658.
[28] T.R. Patel, D. Nikodemus, T.M. Besong, R. Reuten, M. Meier, S.E. Harding, D.J. Winzor, M. Koch, J. Stetefeld, Biophysical analysis of a lethal laminin alpha-1 mutation reveals altered self-interaction, Matrix Biol. 49 (2016) 93–105.
[29] P. Schuck, Analytical ultracentrifugation as a tool for studying protein interactions, Biophys. Rev. 5 (2) (2013) 159–171.

[30] T.C. Yang, C.E. Catalano, N.K. Maluf, Analytical ultracentrifugation as a tool to study nonspecific protein-DNA interactions, Methods Enzymol. 562 (2015) 305–330.
[31] T.R. Patel, S.E. Harding, A. Ebringerova, M. Deszczynski, Z. Hromadkova, A. Togola, B.S. Paulsen, G.A. Morris, A.J. Rowe, Weak self-association in a carbohydrate system, Biophys. J . 93 (3) (2007) 741–749.
[32] N. Wenta, U. Vinkemeier, Characterization of STAT self-association by analytical ultracentrifugation, Methods Mol. Biol. 967 (2013) 203–224.
[33] J.D. Salter, J. Krucinska, J. Raina, H.C. Smith, J.E. Wedekind, A hydrodynamic analysis of APOBEC3G reveals a monomer-dimer-tetramer self-association that has implications for anti-HIV function, Biochemistry 48 (45) (2009) 10685–10687.
[34] T.M. Laue, W.F. Stafford III, Modern applications of analytical ultracentrifugation, Annu. Rev. Biophys. Biomol. Struct. 28 (1) (1999) 75–100.
[35] H. Fujita, Foundations of Ultracentrifugal Analysis, Wiley, New York, 1975.
[36] O. Lamm, Die Differentialgleichung der Ultrazentrifugierung, Arkiv for Matematik, Astronomi och Fysik utgifvet af K. Svenska Vetenskaps-Akademien 21B (1929) 1–4.
[37] G. Ralston, Introduction to Analytical Ultracentrifugation, Beckman Instruments, Inc., Fullerton, 1993.
[38] P. Kratochvil, U.W. Suter, Definitions of terms relating to individual macromolecules, their assemblies, and dilute polymer-solutions, Pure Appl. Chem. 61 (1989) 211–241.
[39] S.E. Harding, Challenges for the modern analytical ultracentrifuge analysis of polysaccharides, Carbohydr. Res. 340 (5) (2005) 811–826.
[40] S.E. Harding, G. Berth, A. Ball, J.R. Mitchell, J.G. de la Torre, The molecular weight distribution and conformation of citrus pectins in solution studied by hydrodynamics, Carbohydr. Polym. 16 (1) (1991) 1–15.
[41] R.B. Gillis, G.G. Adams, D.T. Besong, E. Machova, A. Ebringerova, A.J. Rowe, S.E. Harding, T.R. Patel, Application of novel analytical ultracentrifuge analysis to solutions of fungal mannans, Eur. Biophys. J. (2016).
[42] J.R. Chittuluru, Y. Chaban, J. Monnet-Saksouk, M.J. Carrozza, V. Sapountzi, W. Selleck, J. Huang, R.T. Utley, M. Cramet, S. Allard, G. Cai, J.L. Workman, M.G. Fried, S. Tan, J. Cote, F.J. Asturias, Structure and nucleosome interaction of the yeast NuA4 and Piccolo-NuA4 histone acetyltransferase complexes, Nat. Struct. Mol. Biol. 18 (11) (2011) 1196–1203.
[43] T.C. Pearce, A.J. Rowe, G. Turnock, Determination of molecular-weights of rnas by low-speed sedimentation equilibrium – 16-S ribosomal-Rna as a model compound, J. Mol. Biol. 97 (2) (1975) 193–201.
[44] J.E. Ramsey, M.A. Daugherty, R.J. Kelm Jr., Hydrodynamic studies on the quaternary structure of recombinant mouse Purbeta, J. Biol. Chem. 282 (3) (2007) 1552–1560.
[45] J.W. Ucci, J.L. Cole, Global analysis of non-specific protein-nucleic interactions by sedimentation equilibrium, Biophys. Chem. 108 (1-3) (2004) 127–140.
[46] P. Hensley, Defining the structure and stability of macromolecular assemblies in solution: the re-emergence of analytical ultracentrifugation as a practical tool, Structure 4 (4) (1996) 367–373.
[47] S.E. Harding, K.M. Varum, B.T. Stokke, O. Smidsrod, Molecular weight determination of polysaccharides, in: C.A. White (Ed.), Advances in Carbohydrate Analysis, 1991, pp. 63–114.
[48] J.M. Creeth, R.H. Pain, The determination of molecular weights of biological macromolecules by ultracentrifuge methods, Prog. Biophys. Mol. Biol. 17 (1967) 217–287.
[49] J. Cole, J. Hansen, Analytical ultracentrifugation as a contemporary biomolecular research tool, J. Biomol. Tech. 10 (4) (1999) 163–176.
[50] Y.V. Sergeev, M.B. Dolinska, P.T. Wingfield, Thermodynamic analysis of weak protein interactions using sedimentation equilibrium, Curr. Protoc. Protein Sci. 77 (2014) 20.13.1–20.13.15.
[51] S. Deo, T.R. Patel, E. Dzananovic, E.P. Booy, K. Zeid, K. McEleney, S.E. Harding, S.A. McKenna, Activation of 2′ 5′-oligoadenylate synthetase by stem loops at the 5′-end of the West Nile virus genome, PLoS ONE 9 (3) (2014) e92545.
[52] T.R. Patel, M. Meier, J. Li, G. Morris, A.J. Rowe, J. Stetefeld, T-shaped arrangement of the recombinant agrin G3-IgG Fc protein, Protein Sci. 20 (6) (2011) 931–940.
[53] T.R. Patel, D.R. Picout, S.B. Ross-Murphy, S.E. Harding, Pressure cell assisted solution characterization of galactomannans. 3. Application of analytical ultracentrifugation techniques, Biomacromolecules 7 (12) (2006) 3513–3520.
[54] T.R. Patel, G.A. Morris, J.G. de la Torre, A. Ortega, P. Mischnick, S.E. Harding, Molecular flexibility of methylcelluloses of differing degree of substitution by combined sedimentation and viscosity analysis, Macromol. Biosci. 8 (12) (2008) 1108–1115.
[55] T.R. Patel, G.A. Morris, A. Ebringerová, M. Vodeničarová, V. Velebný, A. Ortega, J. Garcia de la Torre, S.E. Harding, Global conformation analysis of irradiated xyloglucans, Carbohydr. Polym. 74 (4) (2008) 845–851.
[56] W.A. Al-Zyoud, R.M. Hynson, L.A. Ganuelas, A.C. Coster, A.P. Duff, M.A. Baker, A.G. Stewart, E. Giannoulatou, J.W. Ho, K. Gaus, D. Liu, L.K. Lee, T. Bocking, Binding of transcription factor GabR to DNA requires recognition of DNA shape at a location distinct from its cognate binding site, Nucleic Acids Res. 44 (3) (2016) 1411–1420.
[57] M. Resch, Y. Gopel, B. Gorke, R. Ficner, Crystallization and preliminary X-ray diffraction analysis of YhbJ from Escherichia coli, a key protein involved in the GlmYZ sRNA regulatory cascade, Acta Crystallogr., Sect. F: Struct. Biol. Cryst. Commun. 69 (Pt 2) (2013) 109–114.
[58] C.A. Brautigam, Using Lamm-Equation modeling of sedimentation velocity data to determine the kinetic and thermodynamic properties of macromolecular interactions, Methods 54 (1) (2011) 4–15.
[59] S.E. Harding, A.J. Rowe, Insight into protein-protein interactions from analytical ultracentrifugation, Biochem. Soc. Trans. 38 (4) (2010) 901–907.
[60] A. Le Roy, K. Wang, B. Schaack, P. Schuck, C. Breyton, C. Ebel, AUC and small-angle scattering for membrane proteins, Methods Enzymol. 562 (2015) 257–286.
[61] J. Liu, S. Yadav, J. Andya, B. Demeule, S.J. Shire, Analytical ultracentrifugation and its role in development and research of therapeutical proteins, Methods Enzymol. 562 (2015) 441–476.
[62] S.J. Perkins, R. Nan, K. Li, S. Khan, Y. Abe, Analytical ultracentrifugation combined with X-ray and neutron scattering: experiment and modelling, Methods 54 (1) (2011) 181–199.
[63] J.W. Strutt LVIII, On the scattering of light by small particles, Philosophical Magazine Series 4 41 (275) (1871) 447–454.
[64] J. Tyndall, On the blue colour of the sky, the polarization of skylight, and on the polarization of light by cloudy matter generally, Proc. R. Soc. London 17 (1868) 223–233.
[65] A. Einstein, Über einen die Erzeugung und Verwandlung des Lichtes betreffenden heuristischen Gesichtspunkt, Ann. Phys. 322 (6) (1905) 132–148.
[66] G. Mie, Beiträge zur Optik trüber Medien, speziell kolloidaler Metallösungen, Ann. Phys. 330 (3) (1908) 377–445.
[67] A. Einstein, Zur Theorie der Brownschen Bewegung, Ann. Phys. 324 (2) (1906) 371–381.
[68] W. Sutherland LXXV, A dynamical theory of diffusion for non-electrolytes and the molecular mass of albumin, Philosophical Magazine Series 6 9 (54) (1905) 781–785.
[69] S.E. Harding, K. Jumel, Light Scattering, in: J.E. Coligan, B.D. Dunn, H.L. Ploegh, D.W. Speicher, P. T. Wingfield (Eds.), Current Protocols in Protein Science, New York, New York, 1998, pp. 7.8.1–7.8.14.
[70] P.J. Wyatt, Light scattering and the absolute characterization of macromolecules, Anal. Chim. Acta 272 (1) (1993) 1–40.
[71] V.A. Bloomfield, Quasi-elastic light scattering applications in biochemistry and biology, Annu. Rev. Biophys. Bioeng. 10 (1981) 421–450.
[72] S. Fujime, Quasi-elastic scattering of laser light. A new tool for the dynamic study of biological macromolecules, Adv. Biophys. 3 (1972) 1–43.
[73] P.N. Pusey, Correlation and light beating spectroscopy, in: H.Z. Cummings, E. R. Pike (Eds.), Photon Correlation and Light Beating Spectroscopy, Plenum Press, New York, 1974, pp. 387–428.
[74] C. Tanford, Physical Chemistry of Macromolecules, John Wiley & Sons Inc., New York, 1961.
[75] P. Zakharov, F. Scheffold, Advances in dynamic light scattering techniques, in: K. Alexander (Ed.), Light Scattering Reviews 4: Single Light Scattering and Radiative Transfer, Springer Berlin Heidelberg, Heidelberg, 2009, pp. 433–467.
[76] K.E. Van Holde, Physical characterization of the protein molecule, Mol. Biol. Biochem. Biophys. 8 (1970) 2–24.
[77] I.N. Serdyuk, N.R. Zaccai, N. Zaccai, Methods in Molecular Biophysics: Structure, Dynamics, Function, Cambridge University Press, Cambridge, 2007.
[78] U. Nobbmann, M. Connah, B. Fish, P. Varley, C. Gee, S. Mulot, J. Chen, L. Zhou, Y. Lu, F. Shen, J. Yi, S.E. Harding, Dynamic light scattering as a relative tool for assessing the molecular integrity and stability of monoclonal antibodies, Biotechnol. Genet. Eng. Rev. 24 (2007) 117–128.
[79] B. Lorber, F. Fischer, M. Bailly, H. Roy, D. Kern, Protein analysis by dynamic light scattering: methods and techniques for students, Biochem. Mol. Biol. Educ. 40 (6) (2012) 372–382.
[80] S.E. Harding, Classical Light Scattering for the determination of molecular weight and gross conformation of biological macromolecules, in: C. Jones, B. Mulloy, A. Thomas (Eds.), Methods in Molecular Biology, Humana Press, New Jercy, 1994, pp. 85–95.
[81] P.J. Wyatt, Combined differential light scattering with gel permeation chromatography for the molecular weight determination, in: S.E. Harding, D.B. Sattelle, V.A. Bloomfield (Eds.), Laser Light Scattering in Biochemistry, Royal Society of Chemistry, Cambridge, United Kingdom, 1992, pp. 35–58.
[82] S. Girod, P. Baldet-Dupy, H. Maillols, J.-M. Devoisselle, On-line direct determination of the second virial coefficient of a natural polysaccharide using size-exclusion chromatography and multi-angle laser light scattering, J. Chromatogr. A 943 (1) (2002) 147–152.
[83] P. Debye, Light scattering in solutions, J. Appl. Phys. 15 (4) (1944) 338–342.
[84] B.H. Zimm, Molecular theory of the scattering of light in fluids, J. Chem. Phys. 13 (4) (1945) 141–145.
[85] B.H. Zimm, The scattering of light and the radial distribution function of high polymer solutions, J. Chem. Phys. 16 (12) (1948) 1093–1099.
[86] M.A. Talavera, E.E. Matthews, W.K. Eliason, I. Sagi, J. Wang, A. Henn, E.M. De La Cruz, Hydrodynamic characterization of the DEAD-box RNA helicase DbpA, J. Mol. Biol. 355 (4) (2006) 697–707.
[87] M. Fislage, E. Brosens, E. Deyaert, A. Spilotros, E. Pardon, R. Loris, J. Steyaert, A. Garcia-Pino, W. Versees, SAXS analysis of the tRNA-modifying enzyme complex MnmE/MnmG reveals a novel interaction mode and GTP-induced oligomerization, Nucleic Acids Res. 42 (9) (2014) 5978–5992.
[88] M.P. Benoit, L. Imbert, A. Palencia, J. Perard, C. Ebel, J. Boisbouvier, M.J. Plevin, The RNA-binding region of human TRBP interacts with microRNA precursors through two independent domains, Nucleic Acids Res. 41 (7) (2013) 4241–4252.
[89] C. Zhao, A.M. Pyle, Crystal structures of a group II intron maturase reveal a missing link in spliceosome evolution, Nat. Struct. Mol. Biol. 23 (6) (2016) 558–565.

[90] S.A. Beckham, J. Brouwer, A. Roth, D. Wang, A.J. Sadler, M. John, K. Jahn-Hofmann, B.R. Williams, J.A. Wilce, M.C. Wilce, Conformational rearrangements of RIG-I receptor on formation of a multiprotein:dsRNA assembly, Nucleic Acids Res. 41 (5) (2013) 3436–3445.
[91] C.N. Leettola, M.J. Knight, D. Cascio, S. Hoffman, J.U. Bowie, Characterization of the SAM domain of the PKD-related protein ANKS6 and its interaction with ANKS3, BMC Struct. Biol. 14 (2014) 17.
[92] A. Theisen, C. Johann, M.P. Deacon, S.E. Harding, Refractive Increment Data-book for Polymer and Biomolecular Scientists, Nottingham University Press, Nottingham, United Kingdom, 2000.
[93] B.H. Zimm, Apparatus and methods for measurement and interpretation of the angular variation of light scattering – preliminary results on polystyrene solutions, J. Chem. Phys. 16 (12) (1948) 1099–1116.
[94] S.E. Harding, K.M. Vårum, B.T. Stokke, O. Smidsrød, P.J. Wyatt, Molecular weight determination of polysaccharides, in: C.A. White (Ed.), Advances in Carbohydrate Analysis, 1992, pp. 63–144.
[95] P. Debye, Molecular weight determination by light scattering, J. Phys. Colloidal Chem. 51 (1947) 18–32.
[96] S.E. Harding, D.B. Sattelle, V.A. Bloomfield, Laser-light scattering in biochemistry – introductory-remarks, Biochem. Soc. Trans. 19 (2) (1991). 477–477.
[97] S. Fekete, A. Beck, J.L. Veuthey, D. Guillarme, Theory and practice of size exclusion chromatography for the analysis of protein aggregates, J. Pharm. Biomed. Anal. 101 (2014) 161–173.
[98] R.B. Gillis, A.J. Rowe, G.G. Adams, S.E. Harding, A review of modern approaches to the hydrodynamic characterisation of polydisperse macromolecular systems in biotechnology, Biotechnol. Genet. Eng. Rev. 30 (1-2) (2014) 142–157.
[99] E. Sahin, C.J. Roberts, Size-exclusion chromatography with multi-angle light scattering for elucidating protein aggregation mechanisms, Methods Mol. Biol. 899 (2012) 403–423.
[100] C.E. Blanchet, D.I. Svergun, Small-angle X-ray scattering on biological macromolecules and nanocomposites in solution, Annu. Rev. Phys. Chem. 64 (2013) 37–54.
[101] D.A. Jacques, J. Trewhella, Small-angle scattering for structural biology-expanding the frontier while avoiding the pitfalls, Protein Sci. 19 (4) (2010) 642–657.
[102] C.D. Putnam, M. Hammel, G.L. Hura, J.A. Tainer, X-ray solution scattering (SAXS) combined with crystallography and computation: defining accurate macromolecular structures, conformations and assemblies in solution, Q. Rev. Biophys. 40 (03) (2007) 191–285.
[103] J. Trewhella, Small-angle scattering and 3D structure interpretation, Curr. Opin. Struct. Biol. 40 (2016) 1–7.
[104] D.I. Svergun, M.H. Koch, Advances in structure analysis using small-angle scattering in solution, Curr. Opin. Struct. Biol. 12 (5) (2002) 654–660.
[105] A.T. Tuukkanen, D.I. Svergun, Weak protein-ligand interactions studied by small-angle X-ray scattering, FEBS J. 281 (8) (2014) 1974–1987.
[106] M.A. Graewert, D.I. Svergun, Impact and progress in small and wide angle X-ray scattering (SAXS and WAXS), Curr. Opin. Struct. Biol. 23 (5) (2013) 748–754.
[107] A. Guinier, G. Fourner, Small Angle Scattering of X-Rays, Wiley, New York, 1955.
[108] R.P. Rambo, J.A. Tainer, Accurate assessment of mass, models and resolution by small-angle scattering, Nature 496 (7446) (2013) 477–481.
[109] M.V. Petoukhov, D.I. Svergun, Applications of small-angle X-ray scattering to biomacromolecular solutions, Int. J. Biochem. Cell Biol. 45 (2) (2013) 429–437.
[110] H.D. Mertens, D.I. Svergun, Structural characterization of proteins and complexes using small-angle X-ray solution scattering, J. Struct. Biol. 172 (1) (2010) 128–141.
[111] M.H. Koch, P. Vachette, D.I. Svergun, Small-angle scattering: a view on the properties, structures and structural changes of biological macromolecules in solution, Q. Rev. Biophys. 36 (2) (2003) 147–227.
[112] D. Durand, C. Vives, D. Cannella, J. Perez, E. Pebay-Peyroula, P. Vachette, F. Fieschi, NADPH oxidase activator p67(phox) behaves in solution as a multidomain protein with semi-flexible linkers, J. Struct. Biol. 169 (1) (2010) 45–53.
[113] V. Receveur-Brechot, D. Durand, How random are intrinsically disordered proteins? A small angle scattering perspective, Curr. Protein Pept. Sci. 13 (1) (2012) 55–75.
[114] V.M. Burger, D.J. Arenas, C.M. Stultz, A structure-free method for quantifying conformational flexibility in proteins, Sci. Rep. 6 (2016) 29040.
[115] P.V. Konarev, V.V. Volkov, A.V. Sokolova, M.H.J. Koch, D.I. Svergun, PRIMUS: a Windows PC-based system for small-angle scattering data analysis, J. Appl. Crystallogr. 36 (2003) 1277–1282.
[116] E. Dzananovic, T.R. Patel, S. Deo, K. McEleney, J. Stetefeld, S.A. McKenna, Recognition of viral RNA stem-loops by the tandem double-stranded RNA binding domains of PKR, RNA 19 (3) (2013) 333–344.
[117] A.A. Kermani, R. Roy, G. Gopalasingam, K.I. Kocurek, Y. Zhang, T.R. Patel, A.J. Alderwich, G.S. Besra, K. Fütterer, Crystal and solution structure of the TreS-Pep2 complex, initiating α-glucan synthesis in the GlgE pathway of mycobacteria, Nature Scientific Reports (in preparation).
[118] J. Hennig, C. Militti, G.M. Popowicz, I. Wang, M. Sonntag, A. Geerlof, F. Gabel, F. Gebauer, M. Sattler, Structural basis for the assembly of the Sxl-Unr translation regulatory complex, Nature 515 (7526) (2014) 287–290.
[119] A. Lapinaite, B. Simon, L. Skjaerven, M. Rakwalska-Bange, F. Gabel, T. Carlomagno, The structure of the box C/D enzyme reveals regulation of RNA methylation, Nature 502 (7472) (2013) 519–523.
[120] M. Hengesbach, H. Schwalbe, Structural basis for regulation of ribosomal RNA 2′-O-methylation, Angew. Chem. Int. Ed. Engl. 53 (7) (2014) 1742–1744.
[121] M. Falb, I. Amata, F. Gabel, B. Simon, T. Carlomagno, Structure of the K-turn U4 RNA: a combined NMR and SANS study, Nucleic Acids Res. 38 (18) (2010) 6274–6285.
[122] G. Zaccai, Straight lines of neutron scattering in biology: a review of basic controls in SANS and EINS, Eur. Biophys. J. 41 (10) (2012) 781–787.
[123] G. Zaccai, B. Jacrot, Small angle neutron scattering, Annu. Rev. Biophys. Bioeng. 12 (1983) 139–157.
[124] F. Gabel, Small-angle neutron scattering for structural biology of protein-RNA complexes, Methods Enzymol. 558 (2015) 391–415.
[125] M.V. Petoukhov, D.I. Svergun, Analysis of X-ray and neutron scattering from biomacromolecular solutions, Curr. Opin. Struct. Biol. 17 (5) (2007) 562–571.
[126] T. Carlomagno, Present and future of NMR for RNA-protein complexes: a perspective of integrated structural biology, J. Magn. Reson. 241 (2014) 126–136.
[127] H.S. Kim, F. Gabel, Uniqueness of models from small-angle scattering data: the impact of a hydration shell and complementary NMR restraints, Acta Crystallogr. D Biol. Crystallogr. 71 (Pt 1) (2015) 57–66.
[128] K. Rother, M. Rother, M. Boniecki, T. Puton, J.M. Bujnicki, RNA and protein 3D structure modeling: similarities and differences, J. Mol. Model. 17 (9) (2011) 2325–2336.
[129] W.K. Dawson, J.M. Bujnicki, Computational modeling of RNA 3D structures and interactions, Curr. Opin. Struct. Biol. 37 (2016) 22–28.
[130] J.P. Rodrigues, A.M. Bonvin, Integrative computational modeling of protein interactions, FEBS J. 281 (8) (2014) 1988–2003.
[131] M. Magnus, D. Matelska, G. Lach, G. Chojnowski, M.J. Boniecki, E. Purta, W. Dawson, S. Dunin-Horkawicz, J.M. Bujnicki, Computational modeling of RNA 3D structures, with the aid of experimental restraints, RNA Biol. 11 (5) (2014) 522–536.
[132] E. Karaca, A.M. Bonvin, Advances in integrative modeling of biomolecular complexes, Methods 59 (3) (2013) 372–381.
[133] J.L. MacCallum, A. Perez, K.A. Dill, Determining protein structures by combining semireliable data with atomistic physical models by Bayesian inference, Proc. Natl. Acad. Sci. U.S.A. 112 (22) (2015) 6985–6990.
[134] P.C. Chen, J.S. Hub, Interpretation of solution x-ray scattering by explicit-solvent molecular dynamics, Biophys. J. 108 (10) (2015) 2573–2584.
[135] K.Y. Sanbonmatsu, C.S. Tung, High performance computing in biology: multimillion atom simulations of nanoscale systems, J. Struct. Biol. 157 (3) (2007) 470–480.
[136] V. Tozzini, Multiscale modeling of proteins, Acc. Chem. Res. 43 (2) (2010) 220–230.
[137] Multiscale Approaches to Protein Modeling, Springer-Verlag, New York, New York, 2011.
[138] A. Malhotra, R.K. Tan, S.C. Harvey, Modeling large RNAs and ribonucleoprotein particles using molecular mechanics techniques, Biophys. J . 66 (6) (1994) 1777–1795.
[139] M.J. Sippl, Boltzmann's principle, knowledge-based mean fields and protein folding. An approach to the computational determination of protein structures, J. Comput. Aided Mol. Des. 7 (4) (1993) 473–501.
[140] C. Chothia, A.M. Lesk, The relation between the divergence of sequence and structure in proteins, EMBO J. 5 (4) (1986) 823–826.
[141] O. Duss, M. Yulikov, F.H. Allain, G. Jeschke, Combining NMR and EPR to determine structures of large RNAs and protein-RNA complexes in solution, Methods Enzymol. 558 (2015) 279–331.
[142] G. Gavory, M.F. Symmons, Y. Krishnan Ghosh, D. Klenerman, S. Balasubramanian, Structural analysis of the catalytic core of human telomerase RNA by FRET and molecular modeling, Biochemistry 45 (44) (2006) 13304–13311.
[143] R.A. Riskowski, R.E. Armstrong, N.L. Greenbaum, G.F. Strouse, Triangulating nucleic acid conformations using multicolor surface energy transfer, ACS Nano 10 (2) (2016) 1926–1938.
[144] D. Schneidman-Duhovny, M. Hammel, A. Sali, FoXS: a web server for rapid computation and fitting of SAXS profiles, Nucleic Acids Res. 38 (Web Server issue) (2010) W540–W544.
[145] C.J. Knight, J.S. Hub, WAXSiS: a web server for the calculation of SAXS/WAXS curves based on explicit-solvent molecular dynamics, Nucleic Acids Res. 43 (W1) (2015) W225–W230.
[146] D. Svergun, C. Barberato, M.H.J. Koch, CRYSOL – a program to evaluate x-ray solution scattering of biological macromolecules from atomic coordinates, J. Appl. Crystallogr. 28 (1995) 768–773.
[147] H. Liu, A. Hexemer, P.H. Zwart, The Small Angle Scattering ToolBox (SASTBX): an open-source software for biomolecular small-angle scattering, J. Appl. Crystallogr. 45 (3) (2012) 587–593.
[148] M. Pelikan, G.L. Hura, M. Hammel, Structure and flexibility within proteins as identified through small angle X-ray scattering, Gen. Physiol. Biophys. 28 (2) (2009) 174–189.
[149] P. Bernado, E. Mylonas, M.V. Petoukhov, M. Blackledge, D.I. Svergun, Structural characterization of flexible proteins using small-angle X-ray scattering, J. Am. Chem. Soc. 129 (17) (2007) 5656–5664.
[150] G. Tria, H.D.T. Mertens, M. Kachala, D.I. Svergun, Advanced ensemble modelling of flexible macromolecules using X-ray solution scattering, IUCrJ 2 (2) (2015) 207–217.

[151] D. Franke, D.I. Svergun, DAMMIF, a program for rapid ab-initio shape determination in small-angle scattering, J. Appl. Crystallogr. 42 (2009) 342–346.

[152] D.I. Svergun, Restoring low resolution structure of biological macromolecules from solution scattering using simulated annealing, Biophys. J . 76 (6) (1999) 2879–2886.

[153] J.C. Grigg, Y. Chen, F.J. Grundy, T.M. Henkin, L. Pollack, A. Ke, T box RNA decodes both the information content and geometry of tRNA to affect gene expression, Proc. Natl. Acad. Sci. U.S.A. 110 (18) (2013) 7240–7245.

[154] S. Banerjee, A. Bartesaghi, A. Merk, P. Rao, S.L. Bulfer, Y. Yan, N. Green, B. Mroczkowski, R.J. Neitz, P. Wipf, V. Falconieri, R.J. Deshaies, J.L. Milne, D. Huryn, M. Arkin, S. Subramaniam, 2.3 A resolution cryo-EM structure of human p97 and mechanism of allosteric inhibition, Science 351 (6275) (2016) 871–875.

[155] A. Bartesaghi, A. Merk, S. Banerjee, D. Matthies, X. Wu, J.L. Milne, S. Subramaniam, 2.2 A resolution cryo-EM structure of beta-galactosidase in complex with a cell-permeant inhibitor, Science 348 (6239) (2015) 1147–1151.

[156] X.C. Bai, I.S. Fernandez, G. McMullan, S.H. Scheres, Ribosome structures to near-atomic resolution from thirty thousand cryo-EM particles, Elife 2 (2013) e00461.

[157] W.P. Galej, M.E. Wilkinson, S.M. Fica, C. Oubridge, A.J. Newman, K. Nagai, Cryo-EM structure of the spliceosome immediately after branching, Nature 537 (7619) (2016) 197–201.

[158] R. Wan, C. Yan, R. Bai, G. Huang, Y. Shi, Structure of a yeast catalytic step I spliceosome at 3.4 A resolution, Science 353 (6302) (2016) 895–904.

[159] B. Wiedenheft, G.C. Lander, K. Zhou, M.M. Jore, S.J. Brouns, J. van der Oost, J.A. Doudna, E. Nogales, Structures of the RNA-guided surveillance complex from a bacterial immune system, Nature 477 (7365) (2011) 486–489.

[160] J. Moult, K. Fidelis, A. Kryshtafovych, T. Schwede, A. Tramontano, Critical assessment of methods of protein structure prediction: progress and new directions in round XI, Proteins 84 (Suppl. 1) (2016) 4–14.

[161] J.A. Cruz, M.F. Blanchet, M. Boniecki, J.M. Bujnicki, S.J. Chen, S. Cao, R. Das, F. Ding, N.V. Dokholyan, S.C. Flores, L. Huang, C.A. Lavender, V. Lisi, F. Major, K. Mikolajczak, D.J. Patel, A. Philips, T. Puton, J. Santalucia, F. Sijenyi, T. Hermann, K. Rother, M. Rother, A. Serganov, M. Skorupski, T. Soltysinski, P. Sripakdeevong, I. Tuszynska, K.M. Weeks, C. Waldsich, M. Wildauer, N.B. Leontis, E. Westhof, RNA-Puzzles: a CASP-like evaluation of RNA three-dimensional structure prediction, RNA 18 (4) (2012) 610–625.

[162] Z. Miao, R.W. Adamiak, M.F. Blanchet, M. Boniecki, J.M. Bujnicki, S.J. Chen, C. Cheng, G. Chojnowski, F.C. Chou, P. Cordero, J.A. Cruz, A.R. Ferre-D'Amare, R. Das, F. Ding, N.V. Dokholyan, S. Dunin-Horkawicz, W. Kladwang, A. Krokhotin, G. Lach, M. Magnus, F. Major, T.H. Mann, B. Masquida, D. Matelska, M. Meyer, A. Peselis, M. Popenda, K.J. Purzycka, A. Serganov, J. Stasiewicz, M. Szachniuk, A. Tandon, S. Tian, J. Wang, Y. Xiao, X. Xu, J. Zhang, P. Zhao, T. Zok, E. Westhof, RNA-Puzzles Round II: assessment of RNA structure prediction programs applied to three large RNA structures, RNA 21 (6) (2015) 1066–1084.

[163] N. Eswar, B. John, N. Mirkovic, A. Fiser, V.A. Ilyin, U. Pieper, A.C. Stuart, M.A. Marti-Renom, M.S. Madhusudhan, B. Yerkovich, A. Sali, Tools for comparative protein structure modeling and analysis, Nucleic Acids Res. 31 (13) (2003) 3375–3380.

[164] A. Sali, T.L. Blundell, Comparative protein modelling by satisfaction of spatial restraints, J. Mol. Biol. 234 (3) (1993) 779–815.

[165] N. Guex, M.C. Peitsch, SWISS-MODEL and the Swiss-PdbViewer: an environment for comparative protein modeling, Electrophoresis 18 (15) (1997) 2714–2723.

[166] T. Schwede, J. Kopp, N. Guex, M.C. Peitsch, SWISS-MODEL: an automated protein homology-modeling server, Nucleic Acids Res. 31 (13) (2003) 3381–3385.

[167] A. Kolinski, Protein modeling and structure prediction with a reduced representation, Acta Biochim. Pol. 51 (2) (2004) 349–371.

[168] M. Blaszczyk, M. Jamroz, S. Kmiecik, A. Kolinski, CABS-fold: server for the de novo and consensus-based prediction of protein structure, Nucleic Acids Res. 41 (Web Server issue) (2013) W406–W411.

[169] K.T. Simons, C. Kooperberg, E. Huang, D. Baker, Assembly of protein tertiary structures from fragments with similar local sequences using simulated annealing and Bayesian scoring functions, J. Mol. Biol. 268 (1) (1997) 209–225.

[170] D.E. Kim, D. Chivian, D. Baker, Protein structure prediction and analysis using the Robetta server, Nucleic Acids Res. 32 (Web Server issue) (2004) W526–W531.

[171] A. Roy, A. Kucukural, Y. Zhang, I-TASSER: a unified platform for automated protein structure and function prediction, Nat. Protoc. 5 (4) (2010) 725–738.

[172] Y. Zhang, I-TASSER server for protein 3D structure prediction, BMC Bioinformatics 9 (2008) 40.

[173] M. Rother, K. Rother, T. Puton, J.M. Bujnicki, ModeRNA: a tool for comparative modeling of RNA 3D structure, Nucleic Acids Res. 39 (10) (2011) 4007–4022.

[174] M. Rother, K. Milanowska, T. Puton, J. Jeleniewicz, K. Rother, J.M. Bujnicki, ModeRNA server: an online tool for modeling RNA 3D structures, Bioinformatics 27 (17) (2011) 2441–2442.

[175] R. Das, D. Baker, Automated de novo prediction of native-like RNA tertiary structures, Proc. Natl. Acad. Sci. U.S.A. 104 (37) (2007) 14664–14669.

[176] M.J. Boniecki, G. Lach, W.K. Dawson, K. Tomala, P. Lukasz, T. Soltysinski, K.M. Rother, J.M. Bujnicki, SimRNA: a coarse-grained method for RNA folding simulations and 3D structure prediction, Nucleic Acids Res. 44 (7) (2016) e63.

[177] M. Magnus, M.J. Boniecki, W. Dawson, J.M. Bujnicki, SimRNAweb: a web server for RNA 3D structure modeling with optional restraints, Nucleic Acids Res. 44 (W1) (2016) W315–W319.

[178] P.B. Moore, Small-angle scattering – information-content and error analysis, J. Appl. Crystallogr. 13 (1980) 168–175.

[179] P.V. Konarev, D.I. Svergun, A posteriori determination of the useful data range for small-angle scattering experiments on dilute monodisperse systems, IUCrJ 2 (Pt 3) (2015) 352–360.

[180] P. Chacon, F. Moran, J.F. Diaz, E. Pantos, J.M. Andreu, Low-resolution structures of proteins in solution retrieved from X-ray scattering with a genetic algorithm, Biophys. J. 74 (6) (1998) 2760–2775.

[181] J. Lipfert, S. Doniach, Small-angle X-ray scattering from RNA, proteins, and protein complexes, Annu. Rev. Biophys. Biomol. Struct. 36 (2007) 307–327.

[182] J. Lipfert, R. Das, V.B. Chu, M. Kudaravalli, N. Boyd, D. Herschlag, S. Doniach, Structural transitions and thermodynamics of a glycine-dependent riboswitch from Vibrio cholerae, J. Mol. Biol. 365 (5) (2007) 1393–1406.

[183] J. Lipfert, V.B. Chu, Y. Bai, D. Herschlag, S. Doniach, Low-resolution models for nucleic acids from small-angle X-ray scattering with applications to electrostatic modeling, J. Appl. Crystallogr. 40 (2007) s229–s234.

[184] D.I. Svergun, M.V. Petoukhov, M.H. Koch, Determination of domain structure of proteins from X-ray solution scattering, Biophys. J. 80 (6) (2001) 2946–2953.

[185] T.R. Patel, R. Reuten, S. Xiong, M. Meier, D.J. Winzor, M. Koch, J. Stetefeld, Determination of a molecular shape for netrin-4 from hydrodynamic and small angle X-ray scattering measurements, Matrix Biol. 31 (2) (2012) 135–140.

[186] J.P. Bacik, M. Tavassoli, T.R. Patel, S.A. McKenna, D.J. Vocadlo, M. Khajehpour, B.L. Mark, Conformational itinerary of Pseudomonas aeruginosa 1,6-anhydro-N-acetylmuramic acid kinase during its catalytic cycle, J. Biol. Chem. 289 (7) (2014) 4504–4514.

[187] E.O. Ariyo, E.P. Booy, T.R. Patel, E. Dzananovic, E.K. McRae, M. Meier, K. McEleney, J. Stetefeld, S.A. McKenna, Biophysical characterization of G-quadruplex recognition in the PITX1 mRNA by the specificity domain of the helicase RHAU, PLoS ONE 10 (12) (2015) e0144510.

[188] G. Vadlamani, M.D. Thomas, T.R. Patel, L.J. Donald, T.M. Reeve, J. Stetefeld, K. G. Standing, D.J. Vocadlo, B.L. Mark, The beta-lactamase gene regulator AmpR is a tetramer that recognizes and binds the D-Ala-D-Ala motif of its repressor UDP-N-acetylmuramic acid (MurNAc)-pentapeptide, J. Biol. Chem. 290 (5) (2015) 2630–2643.

[189] M.V. Petoukhov, D.I. Svergun, Global rigid body modeling of macromolecular complexes against small-angle scattering data, Biophys. J. 89 (2) (2005) 1237–1250.

[190] M.V. Petoukhov, D. Franke, A.V. Shkumatov, G. Tria, A.G. Kikhney, M. Gajda, C. Gorba, H.D. Mertens, P.V. Konarev, D.I. Svergun, New developments in the program package for small-angle scattering data analysis, J. Appl. Crystallogr. 45 (Pt 2) (2012) 342–350.

[191] D. Schneidman-Duhovny, M. Hammel, J.A. Tainer, A. Sali, FoXS, FoXSDock and MultiFoXS: single-state and multi-state structural modeling of proteins and their complexes based on SAXS profiles, Nucleic Acids Res. 44 (W1) (2016) W424–W429.

[192] L.T. Lamech, A.L. Mallam, A.M. Lambowitz, Evolution of RNA-protein interactions: non-specific binding led to RNA splicing activity of fungal mitochondrial tyrosyl-tRNA synthetases, PLoS Biol. 12 (12) (2014) e1002028.

[193] M.E. Birnbaum, R. Berry, Y.S. Hsiao, Z. Chen, M.A. Shingu-Vazquez, X. Yu, D. Waghray, S. Fischer, J. McCluskey, J. Rossjohn, T. Walz, K.C. Garcia, Molecular architecture of the alphabeta T cell receptor-CD3 complex, Proc. Natl. Acad. Sci. U.S.A. 111 (49) (2014) 17576–17581.

[194] V. Haslbeck, J.M. Eckl, A. Drazic, D.A. Rutz, O.R. Lorenz, K. Zimmermann, T. Kriehuber, C. Lindemann, T. Madl, K. Richter, The activity of protein phosphatase 5 towards native clients is modulated by the middle- and C-terminal domains of Hsp90, Sci Rep 5 (2015) 17058.

[195] M. Taube, J.R. Pienkowska, A. Jarmolowski, M. Kozak, Low-resolution structure of the full-length barley (Hordeum vulgare) SGT1 protein in solution, obtained using small-angle X-ray scattering, PLoS ONE 9 (4) (2014) e93313.

[196] W. Wang, H. Hou, Q. Du, W. Zhang, G. Liu, E.V. Shtykova, J. Xu, P. Liu, Y. Dong, Solution small angle X-ray scattering (SAXS) studies of RecQ from Deinococcus radiodurans and its complexes with junction DNA substrates, J. Biol. Chem. 288 (45) (2013) 32414–32423.

[197] S.S. Alqassim, M. Urquiza, E. Borgnia, M. Nagib, L.M. Amzel, M.A. Bianchet, Modulation of MICAL monooxygenase activity by its calponin homology domain: structural and mechanistic insights, Sci. Rep. 6 (2016) 22176.

[198] M.C. Erat, B. Sladek, I.D. Campbell, I. Vakonakis, Structural analysis of collagen type I interactions with human fibronectin reveals a cooperative binding mode, J. Biol. Chem. 288 (24) (2013) 17441–17450.

[199] J. Felix, J. Elegheert, I. Gutsche, A.V. Shkumatov, Y. Wen, N. Bracke, E. Pannecoucke, I. Vandenberghe, B. Devreese, D.I. Svergun, E. Pauwels, B. Vergauwen, S.N. Savvides, Human IL-34 and CSF-1 establish structurally similar extracellular assemblies with their common hematopoietic receptor, Structure 21 (4) (2013) 528–539.

[200] K.H. Tang, M. Niebuhr, A. Aulabaugh, M.D. Tsai, Solution structures of 2: 1 and 1: 1 DNA polymerase-DNA complexes probed by ultracentrifugation and small-angle X-ray scattering, Nucleic Acids Res. 36 (3) (2008) 849–860.

[201] Y.R. Bhandari, W. Jiang, E.A. Stahlberg, J.R. Stagno, Y.X. Wang, Modeling RNA topological structures using small angle X-ray scattering, Methods 103 (2016) 18–24.

[202] X. Fang, J.R. Stagno, Y.R. Bhandari, X. Zuo, Y.X. Wang, Small-angle X-ray scattering: a bridge between RNA secondary structures and three-dimensional topological structures, Curr. Opin. Struct. Biol. 30 (2015) 147–160.
[203] X. Xu, C. Yan, R. Wohlhueter, I. Ivanov, Integrative modeling of macromolecular assemblies from low to near-atomic resolution, Comput. Struct. Biotechnol. J. 13 (2015) 492–503.
[204] Y. Chen, L. Pollack, SAXS studies of RNA: structures, dynamics, and interactions with partners, Wiley Interdiscip. Rev. RNA 7 (4) (2016) 512–526.
[205] R.P. Rambo, Resolving individual components in protein-RNA complexes using small-angle X-ray scattering experiments, Methods Enzymol. 558 (2015) 363–390.
[206] J. Hennig, M. Sattler, The dynamic duo: combining NMR and small angle scattering in structural biology, Protein Sci. 23 (6) (2014) 669–682.
[207] N. Sibille, P. Bernado, Structural characterization of intrinsically disordered proteins by the combined use of NMR and SAXS, Biochem. Soc. Trans. 40 (5) (2012) 955–962.
[208] R.P. Rambo, J.A. Tainer, Super-resolution in solution X-ray scattering and its applications to structural systems biology, Annu. Rev. Biophys. 42 (2013) 415–441.
[209] B. Madan, J.M. Kasprzak, I. Tuszynska, M. Magnus, K. Szczepaniak, W.K. Dawson, J.M. Bujnicki, Modeling of protein-RNA complex structures using computational docking methods, Methods Mol. Biol. 1414 (2016) 353–372.
[210] I. Tuszynska, D. Matelska, M. Magnus, G. Chojnowski, J.M. Kasprzak, L.P. Kozlowski, S. Dunin-Horkawicz, J.M. Bujnicki, Computational modeling of protein-RNA complex structures, Methods 65 (3) (2014) 310–319.
[211] I. Tuszynska, M. Magnus, K. Jonak, W. Dawson, J.M. Bujnicki, NPDock: a web server for protein-nucleic acid docking, Nucleic Acids Res. 43 (W1) (2015) W425–W430.
[212] D. Schneidman-Duhovny, Y. Inbar, R. Nussinov, H.J. Wolfson, PatchDock and SymmDock: servers for rigid and symmetric docking, Nucleic Acids Res. 33 (Web Server issue) (2005) W363–W367.
[213] G.C. van Zundert, J.P. Rodrigues, M. Trellet, C. Schmitz, P.L. Kastritis, E. Karaca, A.S. Melquiond, M. van Dijk, S.J. de Vries, A.M. Bonvin, The HADDOCK2.2 web server: user-friendly integrative modeling of biomolecular complexes, J. Mol. Biol. 428 (4) (2016) 720–725.
[214] B. Jimenez-Garcia, C. Pons, D.I. Svergun, P. Bernado, J. Fernandez-Recio, PyDockSAXS: protein-protein complex structure by SAXS and computational docking, Nucleic Acids Res. 43 (W1) (2015) W356–W361.
[215] A.G. Kikhney, D.I. Svergun, A practical guide to small angle X-ray scattering (SAXS) of flexible and intrinsically disordered proteins, FEBS Lett. 589 (19 Pt A) (2015) 2570–2577.
[216] M. Krzeminski, J.A. Marsh, C. Neale, W.Y. Choy, J.D. Forman-Kay, Characterization of disordered proteins with ENSEMBLE, Bioinformatics 29 (3) (2013) 398–399.
[217] S. Yang, L. Blachowicz, L. Makowski, B. Roux, Multidomain assembled states of Hck tyrosine kinase in solution, Proc. Natl. Acad. Sci. U.S.A. 107 (36) (2010) 15757–15762.
[218] L.D. Antonov, S. Olsson, W. Boomsma, T. Hamelryck, Bayesian inference of protein ensembles from SAXS data, Phys. Chem. Chem. Phys. 18 (8) (2016) 5832–5838.
[219] B. Rozycki, Y.C. Kim, G. Hummer, SAXS ensemble refinement of ESCRT-III CHMP3 conformational transitions, Structure 19 (1) (2011) 109–116.
[220] J. Garcia de la Torre, A. Ortega, H.E. Perez Sanchez, J.G. Hernandez Cifre, MULTIHYDRO and MONTEHYDRO: conformational search and Monte Carlo calculation of solution properties of rigid or flexible bead models, Biophys. Chem. 116 (2) (2005) 121–128.
[221] J. Garcia de la Torre, J.G. Hernandez Cifre, A. Ortega, R.R. Schmidt, M.X. Fernandes, H.E. Perez Sanchez, R. Pamies, SIMUFLEX: algorithms and Tools for Simulation of the Conformation and Dynamics of Flexible Molecules and Nanoparticles in Dilute Solution, J. Chem. Theory Comput. 5 (10) (2009) 2606–2618.
[222] D. Amoros, A. Ortega, J. Garcia de la Torre, Prediction of hydrodynamic and other solution properties of partially disordered proteins with a simple, Coarse-Grained Model, J. Chem. Theory Comput. 9 (3) (2013) 1678–1685.
[223] A. Ortega, D. Amoros, J. Garcia de la Torre, Prediction of hydrodynamic and other solution properties of rigid proteins from atomic- and residue-level models, Biophys. J. 101 (4) (2011) 892–898.
[224] A. Ortega, J. Garcia de la Torre, Equivalent radii and ratios of radii from solution properties as indicators of macromolecular conformation, shape, and flexibility, Biomacromolecules 8 (8) (2007) 2464–2475.
[225] E. Brookes, P. Vachette, M. Rocco, J. Perez, US-SOMO HPLC-SAXS module: dealing with capillary fouling and extraction of pure component patterns from poorly resolved SEC-SAXS data, J. Appl. Crystallogr. 49 (5) (2016).
[226] E. Brookes, B. Demeler, C. Rosano, M. Rocco, The implementation of SOMO (SOlution MOdeller) in the UltraScan analytical ultracentrifugation data analysis suite: enhanced capabilities allow the reliable hydrodynamic modeling of virtually any kind of biomacromolecule, Eur. Biophys. J. 39 (3) (2010) 423–435.
[227] E. Brookes, M. Rocco, Calculation of hydrodynamic parameters: US-SOMO, in: S. Uchiyama, F. Arisaka, W.F. Stafford III, T.M. Laue (Eds.), Analytical Ultracentrifugation: Instrumentation, Software, and Applications, Springer Japan, Japan, 2016, pp. 169–193.
[228] O. Byron, Introduction: calculation of hydrodynamic parameters, in: S. Uchiyama, F. Arisaka, W.F. Stafford III, T.M. Laue (Eds.), Analytical Ultracentrifugation: Instrumentation, Software, and Applications, Springer Japan, Japan, 2016, pp. 147–167.
[229] J. Garcia de la Torre, The HYDRO Software Suite for the Prediction of Solution Properties of Rigid and Flexible Macromolecules and Nanoparticles, in: S. Uchiyama, F. Arisaka, W.F. Stafford III, T.M. Laue (Eds.), Analytical Ultracentrifugation: Instrumentation, Software, and Applications, Springer Japan, Japan, 2016, pp. 195–217.
[230] E. Dzananovic, A., G. Chojnowski, S. Deo, E.P. Booy, K. McEleney, J.M. Bujnicki, T.R. Patel, S.A. McKenna, Structural integrity of the central stem-loop of adenovirus VAI RNA is essential for PKR inhibition, (in preparation).
[231] S. Beick, C. Schmitz-Linneweber, R. Williams-Carrier, B. Jensen, A. Barkan, The pentatricopeptide repeat protein PPR5 stabilizes a specific tRNA precursor in maize chloroplasts, Mol. Cell. Biol. 28 (17) (2008) 5337–5347.
[232] S. Binder, A. Holzle, C. Jonietz, RNA processing and RNA stability in plant mitochondria, Adv. Plant Biol. 1 (2011) 107–130.
[233] Y. Choquet, 5′ and 3′ ends of chloroplast transcripts can both be stabilised by protein 'caps': a new model for polycistronic RNA maturation, EMBO J. 28 (14) (2009) 1989–1990.
[234] J. Prikryl, M. Rojas, G. Schuster, A. Barkan, Mechanism of RNA stabilization and translational activation by a pentatricopeptide repeat protein, Proc. Natl. Acad. Sci. U.S.A. 108 (1) (2011) 415–420.
[235] E. Delannoy, W.A. Stanley, C.S. Bond, I.D. Small, Pentatricopeptide repeat (PPR) proteins as sequence-specificity factors in post-transcriptional processes in organelles, Biochem. Soc. Trans. 35 (2007) 1643–1647.
[236] K. Okuda, T. Nakamura, M. Sugita, T. Shimizu, T. Shikanai, A pentatricopeptide repeat protein is a site recognition factor in chloroplast RNA editing, J. Biol. Chem. 281 (49) (2006) 37661–37667.
[237] A. Barkan, M. Rojas, S. Fujii, A. Yap, Y.S. Chong, C.S. Bond, I. Small, A combinatorial amino acid code for RNA recognition by pentatricopeptide repeat proteins, PLoS Genet. 8 (8) (2012) e1002910.
[238] J. Pfalz, O.A. Bayraktar, J. Prikryl, A. Barkan, Site-specific binding of a PPR protein defines and stabilizes 5′ and 3′ mRNA termini in chloroplasts, EMBO J. 28 (14) (2009) 2042–2052.
[239] P. Yin, Q. Li, C. Yan, Y. Liu, J. Liu, F. Yu, Z. Wang, J. Long, J. He, H.W. Wang, J. Wang, J.K. Zhu, Y. Shi, N. Yan, Structural basis for the modular recognition of single-stranded RNA by PPR proteins, Nature 504 (7478) (2013) 168–171.
[240] B.S. Gully, N. Cowieson, W.A. Stanley, K. Shearston, I.D. Small, A. Barkan, C.S. Bond, The solution structure of the pentatricopeptide repeat protein PPR10 upon binding atpH RNA, Nucleic Acids Res. 43 (3) (2015) 1918–1926.
[241] S. Meyer, S. Bohme, A. Kruger, H.J. Steinhoff, J.P. Klare, A. Wittinghofer, Kissing G domains of MnmE monitored by X-ray crystallography and pulse electron paramagnetic resonance spectroscopy, PLoS Biol. 7 (10) (2009) e1000212.
[242] A. Scrima, I.R. Vetter, M.E. Armengod, A. Wittinghofer, The structure of the TrmE GTP-binding protein and its implications for tRNA modification, EMBO J. 24 (1) (2005) 23–33.
[243] N. Verstraeten, M. Fauvart, W. Versees, J. Michiels, The universally conserved prokaryotic GTPases, Microbiol. Mol. Biol. Rev. 75 (3) (2011) 507–542. second and third pages of table of contents.
[244] L. Yim, I. Moukadiri, G.R. Bjork, M.E. Armengod, Further insights into the tRNA modification process controlled by proteins MnmE and GidA of Escherichia coli, Nucleic Acids Res. 34 (20) (2006) 5892–5905.
[245] S.M. Villordo, A.V. Gamarnik, Genome cyclization as strategy for flavivirus RNA replication, Virus Res. 139 (2) (2009) 230–239.
[246] J. Donovan, M. Dufner, A. Korennykh, Structural basis for cytosolic double-stranded RNA surveillance by human oligoadenylate synthetase 1, Proc. Natl. Acad. Sci. U.S.A. 110 (5) (2013) 1652–1657.
[247] B. Zhang, H. Dong, D.A. Stein, P.L. Iversen, P.Y. Shi, West Nile virus genome cyclization and RNA replication require two pairs of long-distance RNA interactions, Virology 373 (1) (2008) 1–13.
[248] P.R. Reich, B.G. Forget, S.M. Weissman, RNA of low molecular weight in KB cells infected with adenovirus type 2, J. Mol. Biol. 17 (2) (1966) 428–439.
[249] R.P. O'Malley, T.M. Mariano, J. Siekierka, M.B. Mathews, A mechanism for the control of protein synthesis by adenovirus VA RNAI, Cell 44 (3) (1986) 391–400.
[250] S.A. McKenna, D.A. Lindhout, T. Shimoike, C.E. Aitken, J.D. Puglisi, Viral dsRNA inhibitors prevent self-association and autophosphorylation of PKR, J. Mol. Biol. 372 (1) (2007) 103–113.
[251] R.A. Bhat, P.H. Domer, B. Thimmappaya, Structural requirements of adenovirus VAI RNA for its translation enhancement function, Mol. Cell. Biol. 5 (1) (1985) 187–196.
[252] S. Nanduri, B.W. Carpick, Y. Yang, B.R. Williams, J. Qin, Structure of the double-stranded RNA-binding domain of the protein kinase PKR reveals the molecular basis of its dsRNA-mediated activation, EMBO J. 17 (18) (1998) 5458–5465.